Universitat Autònonoma de Barcelona
Departament de Bioquímica i Biologia Molecular

NEW CONCEPTS FOR ELECTRICAL DETECTION OF BIOMOLECULES

Roberto de la Rica Quesada

Tesi Doctoral

Barcelona, Juny 2007

Aquesta tesi, que porta per títol “New concepts for electrical detection of biomolecules” ha estat realitzada als laboratoris de l’Institut de Microelectrònica de Barcelona – Centre Nacional de Microelectrònica del Consell Superior d’Investigacions Científiques per Roberto de la Rica Quesada sota la direcció de Antoni Baldi Coll i César Fernández Sánchez, Investigadors Ramón y Cajal del mateix centre.

Bellaterra, juny 2007

Antoni Baldi Coll	César Fernández Sánchez
Investigador Ramón y Cajal	Investigador Ramón y Cajal

Aquest treball d’investigació s’ha dut a terme gràcies a la beca FPU de l’aleshores Ministeri d’Educació, Cultura i Esport amb identificador AP2002-2713.

Grup de Transductors Químics – Departament de Micro- i Nanosistemes
Institut de Microelectrònica de Barcelona – Centre Nacional de Microelectrònica
Consell Superior d’Investigacions Científiques
Esfera de la Universitat Autònoma de Barcelona
Campus de la Universitat Autònoma de Barcelona
08193 Bellaterra, Barcelona

Aquest treball s'ha dut a terme sota la tutela de Jaume Farrés Vicén, Professor Titular d'Universitat del departament de Bioquímica i Biologia Molecular de la Universitat Autònoma de Barcelona

Jaume Farrés Vicén

Professor Titular d'Universitat del

Departament de Bioquímica i Biologia Molecular

UAB

PAPERS INCLUDED IN THE THESIS

This thesis is based on the following papers, which are referred to in the text by their Roman numerals:

I Roberto de la Rica, César Fernández-Sánchez, Antonio Baldi. Polysilicon interdigitated electrodes as impedimetric sensors. Electrochemistry Communications, 8, 1239-1244, 2006.

II Roberto de la Rica, Antonio Baldi, César Fernández-Sánchez. Local detection of enzymatic ion generation with polycrystalline silicon interdigitated electrodes and its application to biosensing. Applied Physics Letters, 90, 074102, 2007.

III Roberto de la Rica, César Fernández-Sánchez, Antonio Baldi. Electric preconcentration and detection of latex beads with interdigitated electrodes. Applied Physics Letters, 90, 174104, 2007.

In the **Annex** (page 53), the manuscript of the following work is included:

Roberto de la Rica, César Fernández-Sánchez, Ernest Mendoza, Andreu Llobera, Antonio Baldi. Chemically active nanopatterns with gas transfer lithography.

Als meus pares,

al Toni i al César,

gràcies per creure sempre en mí.

CONTENTS

SUMMARY

This work discusses different aspects related to the design of biosensors and biodetection systems. It describes the fabrication and characterization of particular electric transducers together with the development of new transduction systems and the finding of new methodologies for biomolecule nanoarray fabrication.

Firstly, a new type of impedimetric transducer is presented (I). A two-electrode interdigitated design was chosen, mainly for three reasons. First, this geometry allows the monitoring of both the resistivity and the dielectric constant of a solution, thus making interdigitated electrodes more versatile tools than other kind of transducers. Second, they present short electric field penetration depths, which make them more sensitive to changes occurring close to their surface. This fact enables the monitoring of local changes in the magnitudes of interest. Finally, they are suitable for constructing not only sensors but also actuators. This geometry appears to be useful in dielectrophoresis experiments. One innovation introduced in this thesis is the material chosen to fabricate the electrodes: polycrystalline silicon, also known as polysilicon. Polysilicon can be easily modified to render surfaces with distinct physical and chemical properties, thus making this material an excellent approach for biosensors manufacture, comparable to other approaches like alkanethiol chemisorption on gold electrodes.

The aforementioned interdigitated electrodes were used to test two new transduction principles. The two approaches share a common feature: they rely on the ability of interdigitated electrodes to measure local changes in the electrical properties of the medium where they are immersed. In II, this is used to monitor an enzymatic reaction, and it is shown that the characteristics of measuring local changes at interdigitated electrodes result in a more sensitive

detection. Furthermore, the feasibility of this approach for protein detection is demonstrated by using the enzyme as a label for performing an immunoassay. In III, the interdigitated electrodes act both as a transducer and as an actuator. As an actuator, the electrodes are able to concentrate latex beads at their surface. As a transducer, the presence of the insulating microparticles at their surface results in a change in the geometry of the cell, that can be detected by monitoring either the resitance or the capacitance of the solution. Such device performance is parallel to that of magnetoresistive biosensors, and the proposed transduction principle is envisaged as a suitable alternative to them.

Finally, a fourth work is presented in this thesis (Annex). It shares two features in common with the previous works: the substrate (silicon) and a method for biomolecule immobilization (silanization). However, the applications are somehow different, and cover a wider range. Precisely, a new methodology for low cost, easily available nanopatterning is shown. Features made of silane molecules, with dimensions less than 10 nm are successfully patterned. In the frame of biodetection, this new nanopatterning technique is proposed as an alternative to dip-pen nanolithography in nanoarray manufacture. Moreover, the small dimensions of the obtained patterns pave the way for the achievement of single-molecule nanoarrays.

PREFACE

Nowadays, biomolecule detection is one of the most challenging fields in applied sciences. The reason is obvious: living organisms are made of biomolecules, and the capability of detecting biomolecules translates directly in the capability of monitoring life. The applications of this knowledge are diverse and more and more challenging, provided the recent advances in biotechnology. Man is now able to manipulate life in a way never dreamt before. Transgenic organisms are, perhaps, the most striking example of this manipulation, but without any doubt the star topic of this subject is medicine. The reason is clear: it does not matter who you are, where you live or what your social status is, everybody can get ill and, eve ntually, everybody dies.

Let us give an example of how biomolecule detection can improve our lives. Cancer is a good example of a worrying problem. Cancer is a genetic disease that begins with one or several point variations in a biomolecule called *DNA*, which carries the genetic information of living organisms. These variations are known as *mutations*. Mutations have different origins: they can be inherited or acquired during the organism life. Mutations in DNA translate into the production of mutant *proteins*, which are biomolecules as well. Proteins are the effectors of the cells, and mutations can cause the appearance of proteins with truncated functions with respect to the standard ones. As a consequence, the cell cycle may undergo unregulated and, sooner or later, the cell becomes immortal and a tumor appears.

Now, what can be done to fight cancer? The better way is to detect it before it happens, i.e., the *prognosis*. For instance, people with previous cases of this disease in their families could be genetically mapped in order to check whether they carry inherited mutations. Once they know they have a genetic predisposition to suffer the illness, they could change their habits to prevent cancer appearance. If the prognosis fails, an early *diagnostic* would be a

powerful tool to stop cancer. Routine screening of certain proteins (called *tumor markers*) can be performed in groups having a potential risk of suffering cancer. After diagnostic, a convenient therapy is applied to the patient. Every cancer is different, and the knowledge of the exact mutations in a given patient would allow designing tailored therapies.

Another example: a patient arrives to a hospital showing the typical symptoms of suffering a myocardial infarction (a heart attack). An early diagnosis of this affection can be done by measuring the levels of certain proteins in blood.

These two examples are paradigmatic regarding two types of biomolecule sensing. In the first example, it is not expected that the state of a patient is to change from one day to the other. Thus, samples can be extracted, taken to a clinical laboratory, processed and analyzed by using time-consuming tools. Conversely, for the second example it is crucial to know what is happening at the very moment of the patient arrival to the hospital. There is no time for complicated analysis at specialized facilities. Ideally, a nurse or a doctor should be able to perform a rapid test with a small unprocessed sample, for instance a drop of blood.

The most commonly used analysis systems in clinical laboratories are *ELISAs* (enzyme-linked immunosorbent assay) for protein detection and *PCR* (polymerase chain reaction) for DNA detection. Currently, the great challenge for these detection systems is to become high-throughput, that is, to be able to analyze more samples at the same time with a minimum reagent consumption. These requirements are accomplished by *biomolecule arrays*. By contrast, *sensors* are needed for rapid testing. Despite the need of these analysis tools, there are few examples of commercial devices devoted to this matter. Instrumentally, sensors must confine a whole analysis system in a reduced space. Analytically, they must detect the analyte in a complex sample. *Electrical*

sensors are a promising alternative to overcome these drawbacks. On the one hand, they allow easy integration of the instrumentation, due to their fabrication processes and electrical read-out. On the other hand, they can also be easily integrated in miniaturized electromechanical systems, to render *lab-on-a-chip* or *micro total analysis systems*. These approaches include sample processing and biomolecule detection in the same device.

The aforementioned examples give us an idea of the great benefits that biomolecule detection can contribute to the society, but they are just two among a huge range of applications. This thesis deals with several aspects of this subject, from the design of new sensing tools, to the fabrication of potential platforms for biomolecule detection. Although it is difficult to foresee whether these new concepts will have an impact in the industry (and so, in people's life), they try to put a step forward in the development of efficient tools for biomolecule detection.

INTRODUCTION

The present chapter tries to provide the reader with basic concepts regarding the topics treated in this thesis. These themes have been treated with seriousness, and at the same time, with simplicity. This has been done so they can be understood by a wide range of scientists, regardless their specialty. Herein, repetitions of the contents of the scientific papers presented ahead have been avoided. By contrast, this introduction pretends to grant the reader of this thesis a solid, simple background to understand those works.

This introduction begins explaining what a *biomolecule* is, and which its basic characteristics are. This is important for two reasons. First, biomolecules are targets of biosensors and biodetection systems. Second, they themselves are a part of these devices. This is bound to the next topic: *sensors and detection systems*. This section deals with the core theme of this work. Concepts like biosensor, nanoarray or actuator are defined and placed in an understandable context. Then, some information about different ways to *immobilize* biomolecules onto silicon substrates is provided. This subject is a key step in the fabrication of biodevices. Finally, a short introduction to *impedance spectroscopy* can be found. This topic is important because impedance measurements are involved in the detection approaches presented in this work.

1. BIOMOLECULES: PROTEINS AND NUCLEIC ACIDS[1,2]

The word biomolecule comprises a family of organic compounds that are the result of the metabolism of living organisms. They consist primarily of carbon and hydrogen, although nitrogen, oxygen, phosphorus and sulfur may also appear in their chemical composition. This term is applicable to a wide variety of molecules, ranging from small sugars and hormones to polymers like *nucleic acids* and *proteins*. The latter will be the subject of the present work, and the word biomolecule will be used to refer to either of them. Nucleic acids and proteins have a striking feature that makes them especially useful for analytical purposes: they show high affinities for target molecules. The mechanism of this so called *biorecognition event* is explained in the following paragraphs.

1.1 Proteins: antibodies[3,4]

Antibodies belong to a family of proteins know as *immunoglobulins*. The monomers that consistute antibodies and any other protein are the aminoacids. Antibodies are produced by B lymphocytes or B cells which, in mammals, mature in the bone marrow. Their biological role is related to the immune system of animals: they identify strange molecules and mark them for subsequent destruction. Molecules recognized by antibodies are called *antigens*. Virtually, any molecule external to the living organism can be recognized as an antigen. However, some compounds induce a stronger immune response than others. Particularly, antibodies are especially efficient recognizing other proteins. Proteins have large three-dimensional structures and, as a consequence, offer

different sites for particular antibodies. Each one of these sites is named *epitope*. Thus, a given antigen can have several epitopes.

A more comprehensible picture of the recognition mechanism of antibodies can be extracted from a close inspection of their structure. Figure 1 shows a scheme of an antibody belonging to the class G (commonly known as *IgG* for immnunoglobulin G). These proteins have four subunits: two identical light chains and two identical heavy chains. These subunits associate via disulfide bonds as well as non covalent interactions to form a Y-shape symmetric dimmer. The heavy chain shows an oligosaccharide moiety. Light and heavy chains have *constant regions* and *variable regions*. Constant regions are parts of the antibody that are chemically similar among different antibodies, that is, they have almost the same amino acid sequence. By contrast, variable regions show an amazing chemical variability. This diversity results in the formation of regions with a unique chemical composition and structure for each antibody, which enables its interaction with the target molecule with high affinity and specificity.

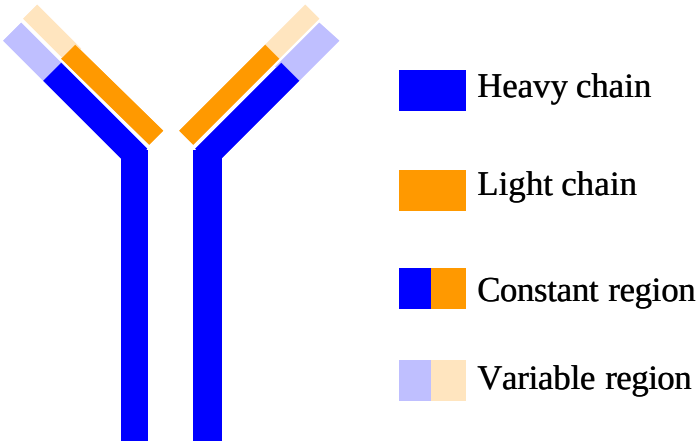

Figure 1. Scheme of an antibody

Once the mechanism of biorecognition event is clearer, the following question arises: how can antibodies be obtained for analytical purposes? Figure 2 shows the answer: inoculating the target protein in an animal, so that its immune system produces the desired antibodies. Let us suppose that the target is a protein

from rabbit. The first step of this process consists in selecting a suitable animal for rising the antibody, that is, an animal of another species, for instance a goat. This ensures that the protein will be recognized by the host as a foreign protein. Following this recognition process, two actions can be performed. On the one hand, the animal can be bled and the serum used without further purification. This serum contains, among others, antibodies against the target protein. Provided that the target may have many epitopes, the resulting serum contains a collection of antibodies that recognize different regions of the analyte. This kind of antibodies is usually known as *polyclonal antibodies*. On the other hand, lymphocytes can be extracted from the animal and fused with cancerous cells to form a *hybridoma*, which mixes the capability of producing antibodies of the original lymphocyte with the immortality of the tumoral cell. These hybridomas are selected and harvested separately, and *monoclonal antibodies* specific for a unique epitope of the protein of interest are obtained.

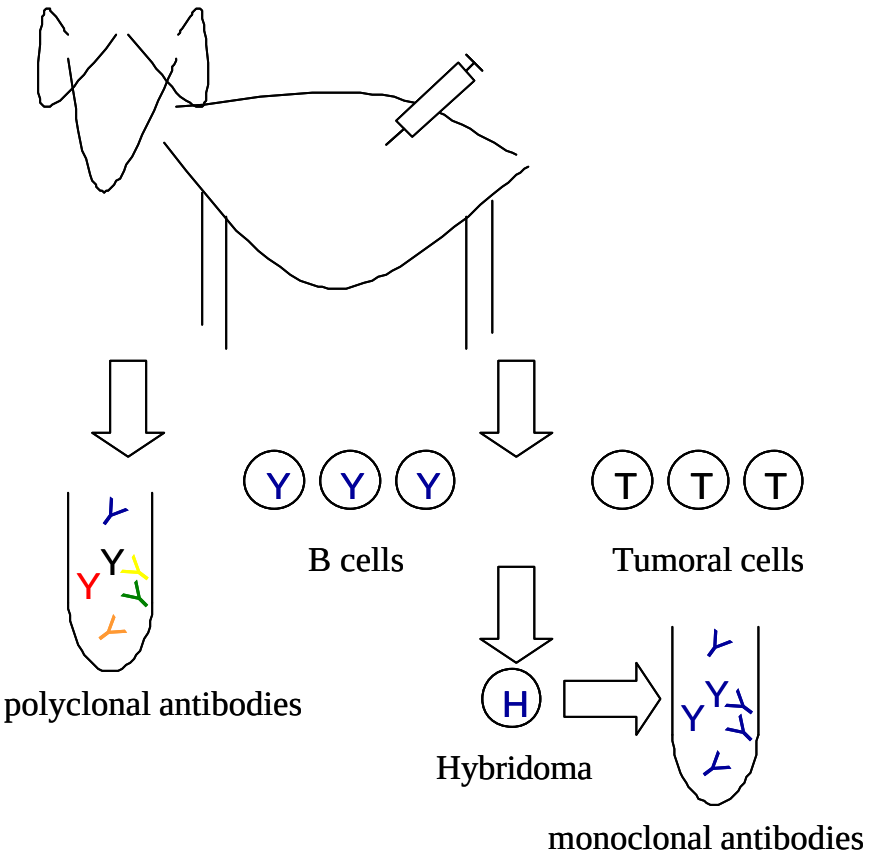

Figure 2. Antibody production.

1.2 Proteins: enzymes[6]

Enzymes are proteins that act as biological catalysts. They differ from ordinary chemical catalysts in several aspects. Firstly, they provide higher reaction rates, typically 10^6 to 10^{12} greater than those of corresponding uncatalyzed reactions and at least several orders of magnitude greater than the corresponding chemically catalyzed reactions. Secondly, enzymatically catalyzed reactions occur under relatively mild conditions. Thirdly, enzymes show greater reaction specificity, that is, enzymatic reactions rarely have side products. Finally, their catalytic activities can be modulated by the presence of molecules other than the reactants.

The region of the enzyme molecule where the catalysis occurs is known as the *active site* of the enzyme. In the active site, the polypeptide chain adopts a conformation suitable for transforming the reactant, also known as the *substrate*. Actually, enzymes can be envisaged as nanoreactors, which are perfectly designed to perform a chemical reaction. Both physical interactions and steric hindrances are responsible for the specificity of the enzymes towards a given substrate. In some enzymes this recognition event takes place at the active site, whereas in other cases it triggers a conformational change that exposes the active site to the substrate. In the active site, certain reactive groups are placed in the proper way to undergo a chemical reaction. Thus, regardless conventional chemical reactions, where the molecules have to collide by diffusion to react, in the enzyme active site everything is pre-arranged to yield the reaction with a smaller energy barrier.

Enzymes have been used as *labels* in biomolecule detection for many decades. For example, they can be easily attached to antibodies with well known chemical procedures. The resulting conjugates mix the specificity of the antibody to recognize target proteins with the amplification provided by the enzymatic reaction. This amplification factor is due to the catalytic properties of the enzyme: high amounts of products are generated by a minimum amount of enzyme (and thus, of analyte). The products of the enzymatic reaction may induce a change in a measurable parameter, either by themselves or linked to other chemical reactions. Some examples of measurable parameters are pH[7,8], conductivity[9], absorbance of a colored product[10], and electrical current[11].

1.3 Nucleic acids: deoxyribonucleic acid or DNA[12]

DNA is the carrier of genetic information in cells and many viruses. DNA often presents a double helical structure. Each strand of the double helix is known as *single-stranded DNA* or *ssDNA*. The building blocks of DNA are *nucleotides*. Each nucleotide consists of three portions: a heterocyclic base, a sugar and a phosphate group. The phosphate group is acidic at physiological pH's and, as a consequence, DNA molecules are negatively charged. There are four kinds of nitrogenous bases: guanine (G), adenine (A), thymine (T) and cytosine (C). The ordered enumeration of nucleotides of a ssDNA molecule is named its *sequence*.

Adenine and guanine, and thymine and cytosine, respectively, are chemically complementary, that is, they recognize and interact with each other (Figure 3). Thus, when two complementary sequences of ssDNA find each other under favorable conditions they form a *double-stranded DNA molecule (dsDNA)*, in a process termed *hybridization*. This self-assembly process is reversible. As a

consequence, particular ssDNA strands are excellent candidates to specifically recognize complementary DNA sequences among other unrelated molecules.

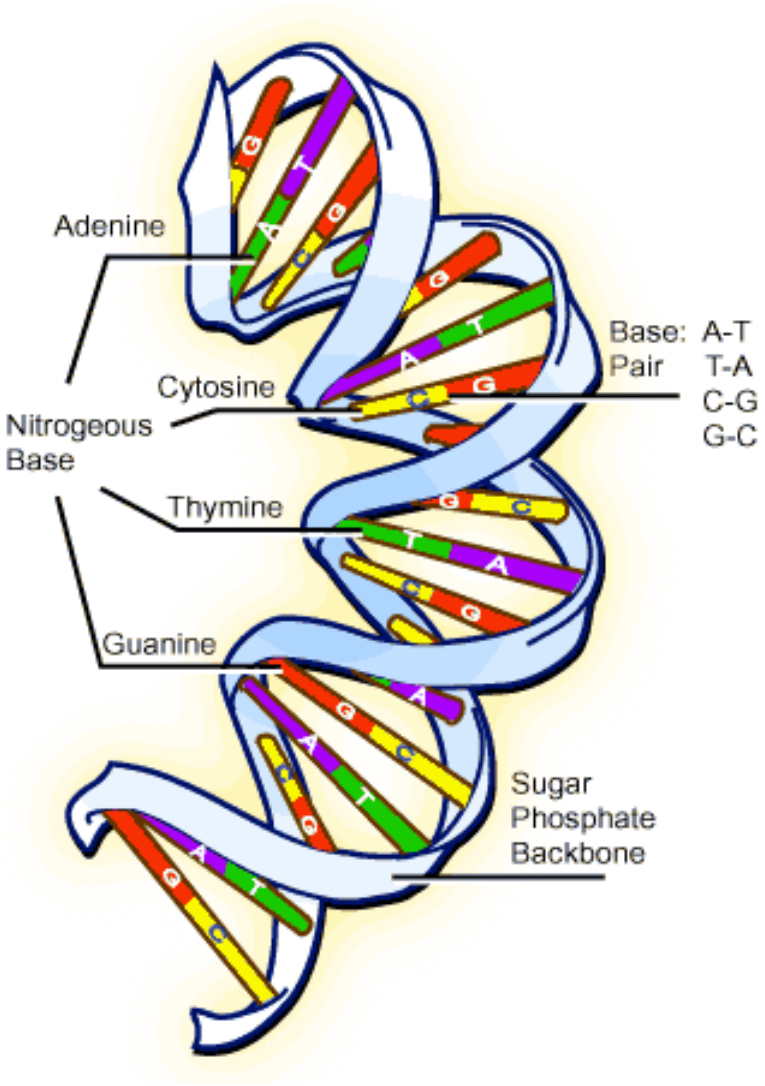

Figure 3. Scheme of a double stranded DNA molecule.

Short DNA molecules are usually referred as *oligonucleotides*. Synthetic oligonucleotides can be easily obtained from many suppliers. They are cheap and custom made, that is, they are synthesized according to the sequence requested by the client. This ease of access to a wide variety of different oligonucleotides is responsible for the extended use of these biomolecules in high throughput detection systems, like *DNA microarrays*[13].

2. DETECTION SYSTEMS, SENSORS, ACTUATORS.

2.1 Detection systems and sensors[14-17]

The barrier between a detection system and a sensor is somehow thin, and often depends on the application envisaged for these two analytical tools. It would be difficult to provide a definition of what a sensor is, which could be applied to all the devices found in the literature under this name. However, some important aspects can be pointed out. Firstly, sensors are analytical devices intended to be used by unskilled staff. As a consequence, the information they render should be easily interpreted. Another feature that describes a sensor approach is its use in decentralized studies, which implies it must be robust. Related to this, a sensor needs to be portable and then it is required to be miniaturized. Overall, a sensor is a customized analytical device, usable by anyone, ready to render fast and direct analytical information about a particular analyte. By contrast, a detection system is used in a laboratory by analytical chemists, can be adapted to measure a wide variety of samples, and the data it provides often needs further processing to become useful information.

An important part of a sensor is the *transducer*. The transducer converts a change in a magnitude into a measurable signal. *Physical sensors* are concerned with measuring physical quantities as length, weight, pressure, and electrical current. A *chemical sensor* is a device that responds to a particular analyte in a selective way through a chemical reaction and can be used for the qualitative or quantitative determination of the analyte. Selectivity can be attained due to the intrinsic chemical properties of the material used to manufacture the sensor, or by the application of a recognition element in close contact with the transducer. When the recognition element is a biomolecule, the resulting device is termed *biosensor*.

The key steps for designing biosensors are:

- A suitable transduction system: in other words, which magnitude is intended to change in the presence of a biorecognition event?

- A suitable transducer: a device able to measure the magnitudes of interest, which is also a good platform for attaching the recognition element.

- A suitable method of biomolecule immobilization: that is, for immobilizing the recognition element. This must be efficient and adapted to the requirements imposed by the transduction system.

It is clear that the three points of this list are intimately related, and people that design sensors always have to keep in mind the final device and its usage when dealing with this subject.

2.2 Immunosensors and immnodetection systems[18].

The prefix immuno- refers to a family of biosensors and detection systems whose recognition element is an antibody. In general, there are three ways of measuring the analyte (Figure 4). In a *sandwich assay*, a primary antibody is used to specifically attach the analyte to the sensor surface. Then, a secondary antibody conjugated to a label (e.g. an enzyme, a fluorochrome, a redox probe) recognizes a specific epitope in the target and provides a measurable signal. Sometimes, the analyte is detected without using a secondary antibody and the assay is simply termed *direct assay*. This can be performed in two ways. On the

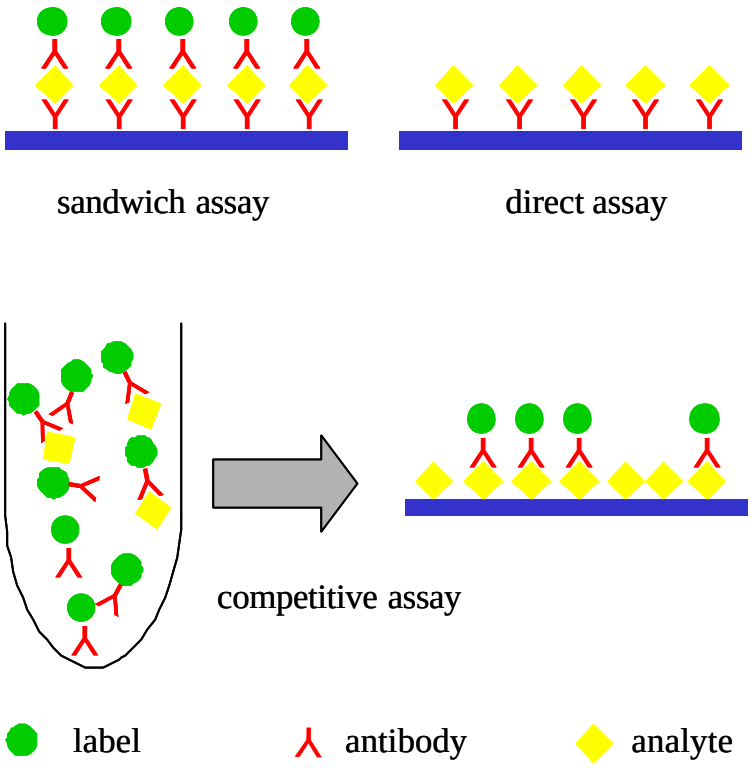

Figure 4. Types of immnunoassays.

one hand, the presence of the analyte may be detected by its intrinsic properties without further labeling. The corresponding detection system or biosensor is said to be *label-free*. On the other hand, the whole sample (including the analyte) may be modified with a label. Provided the high specificity of the attached antibody, only the analyte will be detected after appropriate washing steps to remove the unbound species. This approach has been mostly used in protein microarrays, a term that will be explained in the following section. The third option consists in performing a *competitive assay*. The molecule to be detected is attached to the sensor surface. An excess amount of anti-analyte antibody is added to the sample. The mixture is put in contact with the sensor, so that the free antibodies (the ones that did not react with the analyte) react with the surface. In this case the signal is inverted: the more analyte is present in the sample, the more antibodies it binds and the smaller signal is obtained.

2.3 Bioarrays[19-26]

Bioarrays are high-throughput detection systems that share a common feature with biosensors: the biomolecules that act as recognition elements are attached to a supporting substrate. However, this supporting substrate is not always the sensing element of the detection system. The most extended form of bioarray uses glass slides, where the biomolecules are printed at defined sites. Each resulting microspot has a different recognition element, so that a mixture of analytes can be analyzed at the same time by exposing the whole array to the sample. Tens of thousands of spots can constitute a bioarray, thus showing the challenging opportunities that this kind of detection systems provide.

A special type of bioarray is the *nanoarray*. Protein nanoarrays have been mainly developed by Mirkin and co-workers by using a printing technique called *dip-pen nanolithography*[27-30]. In this case, active sites that interact with proteins are generated by inking the tip of an *atomic force microscope (AFM)* with reactive molecules and drawing a pattern on a substrate. These patterns have physicochemical affinity for the biorecognition element, e.g. an antibody[27,28,31]. Alternatively, the biomolecules themselves can be printed directly onto the surface[32]. The result of the interaction between the recognition element and the analyte is detected with an AFM. In some cases, detection is performed label-free by measuring either an increase in roughness or a change in the forces existing between the tip and the surface due to the presence of the analyte[33,34]. Sometimes, the signal is enhanced with secondary antibodies labeled with colloidal gold[35]. This approach has been successfully applied to detect low levels of viral proteins in HIV-infected patients (Figure 5).

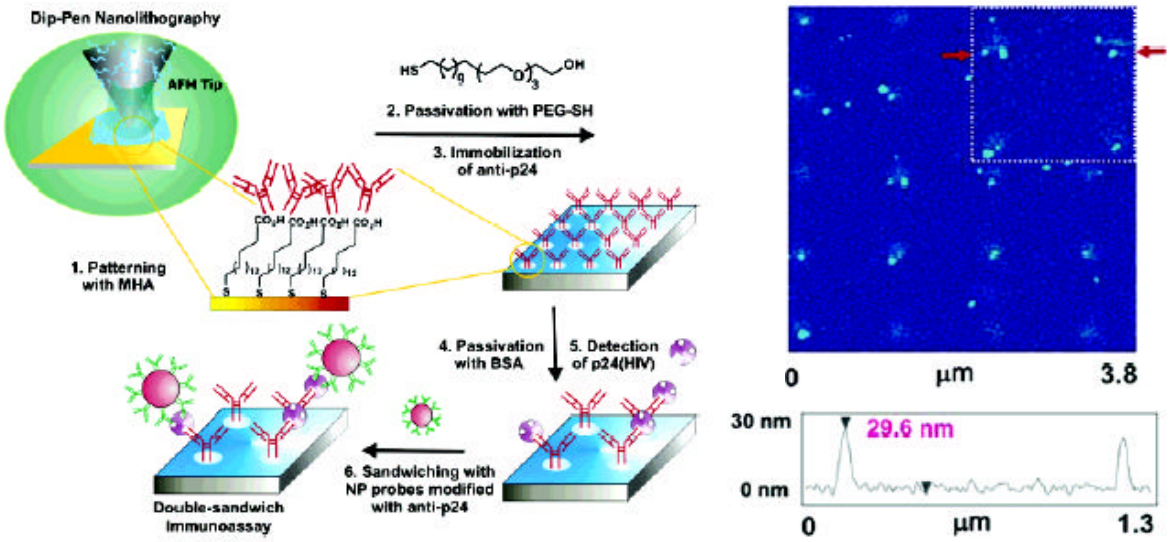

Figure 5. Colloidal gold enhanced AFM detection of HIV antigens.

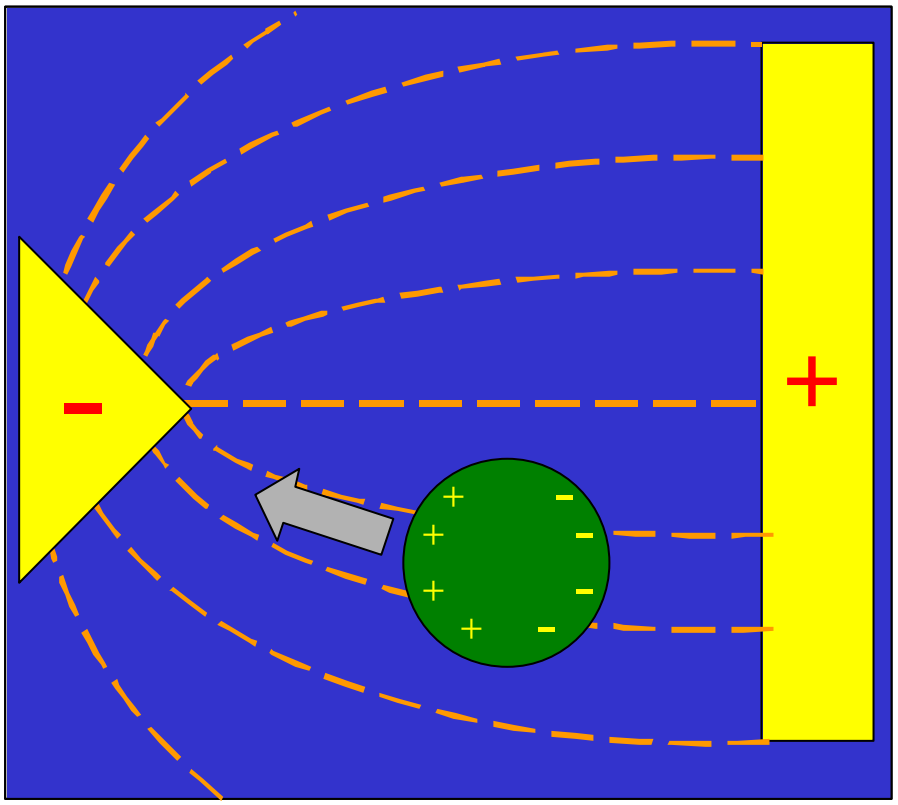

Figure 6. Dielectrophoresis

2.4 Actuators[36]

Actuators are devices for moving or controlling a system. These devices transform an input energy or primary power in an output power or mechanical work. An example of an actuator is a device capable of moving polarizable particles by means of an alternating current (Figure 6). This process is known as *dielectrophoresis* and can be performed by electrodes arranged in a way that generate a divergent electric field. Dielectrophoretic cages[37,38], intercastellated electrodes[39] and *interdigitated electrodes*[39-42] have been proposed as suitable actuators to perform dielectrophoresis.

Actuators based on dielectrophoresis have been extensively used to move microparticles[43,44] and living cells[45,46], as well as biomolecules[47,48] and nanostructures[49,50]. Detection of the polarizable particles was in all cases performed by a different part of the system.

3. METHODS OF IMMOBILIZATION

Two immobilization methods are of interest in this work:

- *Adsorption*: it involves physical interactions (Van der Waals, hydrophobic, electrostatic forces) between the recognition element and the transducer surface. This process happens spontaneously when the sensor is immersed in a solution containing biomolecules, but can be enhanced by carrying out certain surface treatments.

- *Covalent binding*: when covalent bonds are formed between the biomolecule and the transducer surface.

Each one of these two procedures has its pros and cons. Adsorption is simple and suitable for single-use detection systems. However, the interaction is not fully irreversible and the recognition element might be lost if very stringent washing steps are to be done. By contrast, covalent binding is more laborious but also more reliable. Thus, the final choice greatly depends on the application and the way the sensor is going to be managed.

The choice of an immobilization method also depends on the substrate where it is applied. In this thesis, silicon is the substrate of choice. Silicon spontaneously undergoes an oxidation reaction in contact with oxygen to form a thin layer of silicon oxide named *native oxide*. Alternatively, thin oxide layers on silicon can be obtained with a variety of methods, for example, by placing the silicon in a furnace with oxygen atmosphere at temperatures over 800ºC. The resulting high quality oxide is said to be *thermally grown*, and is thicker and more compact than the native oxide. Whatever its origin, silicon oxide has *silanol* groups on its surface, which are suitable for covalently binding *silane* molecules, in a procedure often referred as *silanization*[51,52] (Figure 7). The

silicon atom is electrophilic and reacts with silanol groups to form *siloxane* bonds. Apart from this common feature, organo-alcoxisilanes bearing a huge variety of functional organic groups are commercially available, which makes these molecules a versatile tool for modifying the chemical and physical properties of silicon oxide[53].

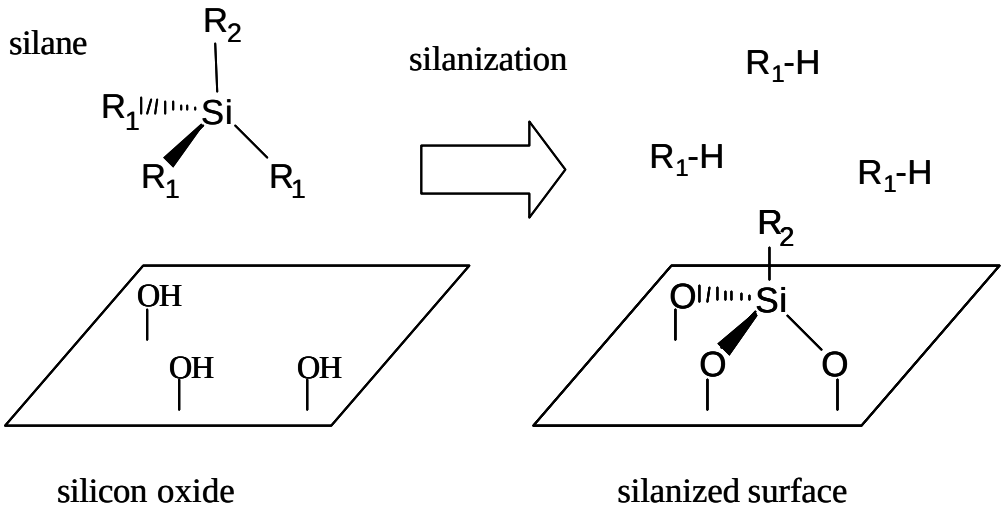

Figure 7. Silanization. Most common R_1 groups are –OCH3, -OCH2CH3, -Cl. A residue R_2 often used in biomolecule attachment is $–CH_2CH_2CH_2NH_2$.

4. IMPEDANCE SPECTROSCOPY

4.1 Impedance theory[54,55]

Impedance refers to the degree in which a system resists the flow of an alternating electrical current upon application of an alternating potential (Equation 1).

$$Z = \frac{E}{I} \qquad \text{(Eq. 1)}$$

Impedance is usually measured using a small sinusoidal excitation signal. This is done so the system is close to the *steady-state* and the response is *pseudo-linear*, even though non-linear elements are present. In a linear system, the current response to a sinusoidal potential will be a sinusoid at the same frequency but shifted in phase (Figure 5).

The excitation signal, expressed as a function of time, has the form

$$E(t) = E_o \cos(wt) \qquad \text{(Eq. 2)}$$

E(t) is the potential at time t, E_0 is the amplitude of the signal, and ω is the radial frequency. In a linear system, the response signal I(t) is shifted in phase (ϕ) and has a different amplitude I_0:

$$I(t) = I_0 \cos(wt - f) \qquad \text{(Eq. 3)}$$

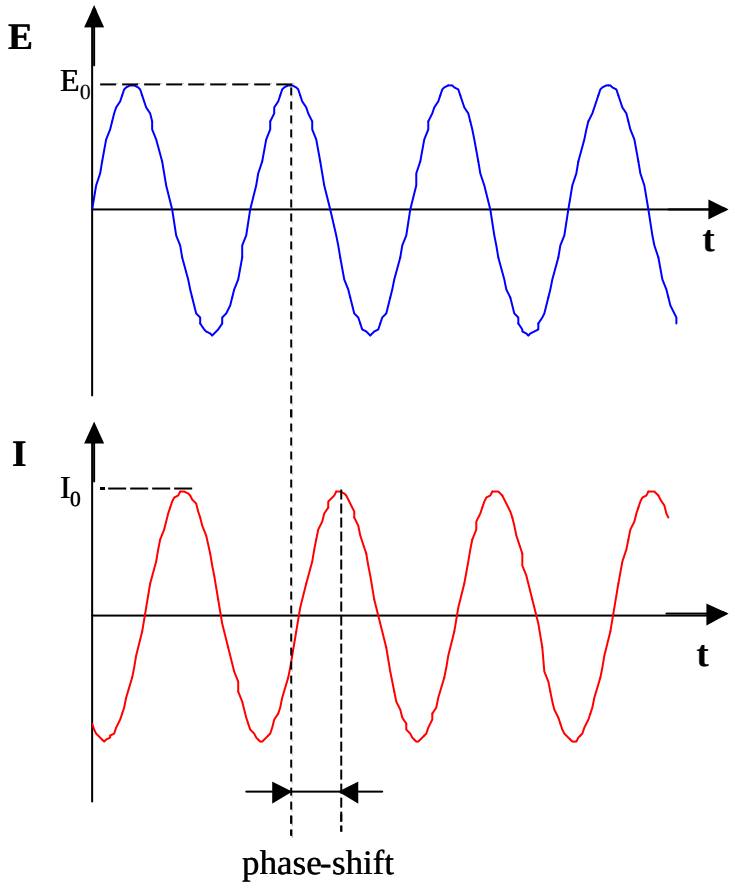

Figure 5. Phase-shift of the output current.

Impedance can be calculated as:

$$Z = \frac{E(t)}{I(t)} = \frac{E_0 \cos(wt)}{I_0 \cos(wt - f)} = Z_0 \frac{\cos(wt)}{\cos(wt - f)} \qquad \text{(Eq. 4)}$$

The impedance is therefore expressed in terms of a magnitude, Z_0 and a phase shift, ϕ. Using Euler relationship, it is possible to express the impedance as a complex function. The potential is described as,

$$E(t) = E_0 \exp(jwt) \quad \text{(Eq. 5)}$$

and the current response as,

$$I(t) = I_0 \exp(jwt - jf) \quad \text{(Eq. 6)}$$

The impedance is then represented as a complex number,

$$Z = \frac{E}{I} = Z_0 \exp(jf) = Z_0(\cos f + j \sin f) \quad \text{(Eq. 7)}$$

$$Z = Z_{real} + Z_{imaginary} = Z' + Z'' \quad \text{(Eq. 8)}$$

Except for purely resistive systems, impedance of a system changes with frequency. The impedance measured for a given range of frequencies is termed *impedance spectrum.* There are two common ways to plot impedance spectra. If the real part of the impedance is plotted on the X axis and the imaginary part on the Y axis of a chart, a *Nyquist plot* is obtained (Figure 6). Notice that in impedance spectroscopy the y-axis usually represents the negative of the imaginary part and that each point on the Nyquist plot is the impedance at one frequency.

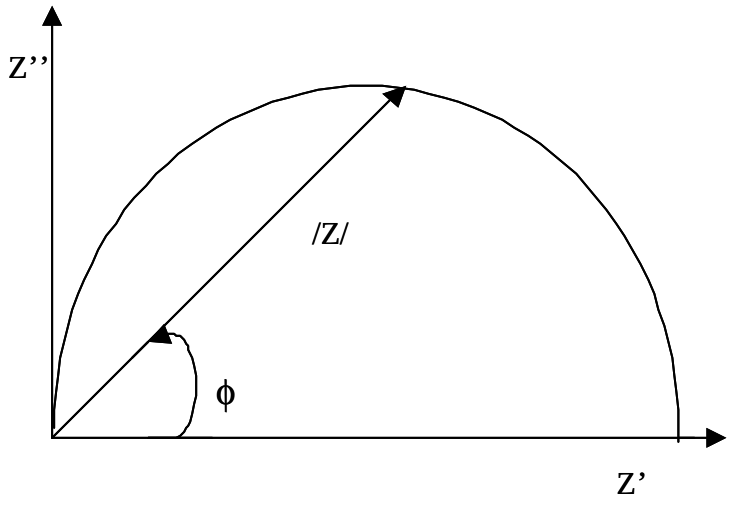

Figure 6. Nyquist plot

On the Nyquist plot the impedance can be represented as a vector of length /Z/. The angle between this vector and the x-axis is ϕ, where $\phi = \arg(Z)$. The representation of /Z/ or ϕ *vs* the frequency in semi logarithmic scale is known as *Bode Plot*.

4. 2 Data fitting

Impedance data is commonly analyzed by fitting them to an equivalent electrical circuit model. Most of the circuit elements in the model are common electrical elements such as *resistors, capacitors,* and *inductors*. An ideal resistor is a circuit component whose impedance is independent of the frequency at which it is measured. The output current is in phase with the input potential, and as a consequence the impedance only has a real component:

Resistor: $\phi = 0$

$/Z/ = Z'$

$Z' = Z$

$Z'' = 0$

For an ideal capacitor:

Capacitor: $\phi = 90^{o}$

$/Z/ = Z''$

$Z' = 0$

$Z'' = Z$

Figure 7 and 8 show an example of the impedance spectrum corresponding to a resistor with a resistance of 1kΩ in parallel with a capacitor of capacitance 1nF:

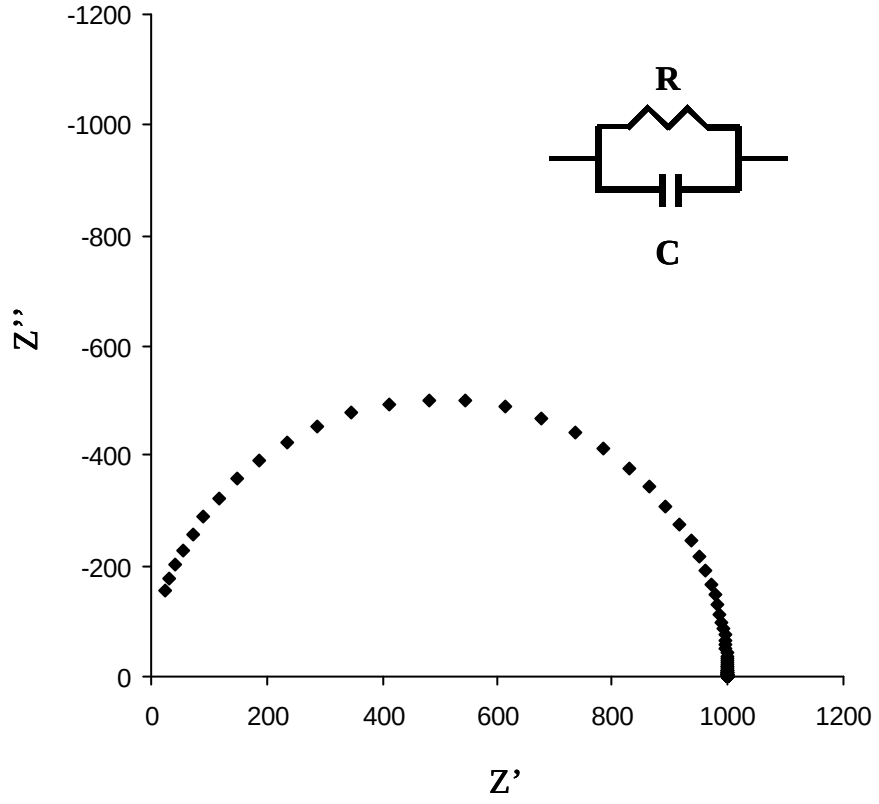

Figure 7. Nyquist plot of the impedance spectrum of a resistor in parallel with a capacitor.

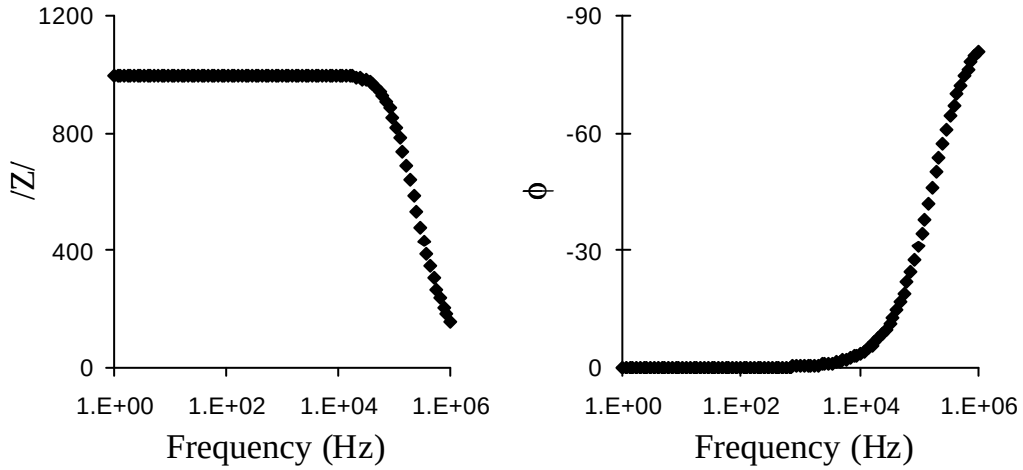

Figure 8. Bode plots of the impedance spectrum of a resistor in parallel with a capacitor.

At high frequencies, the impedance spectrum shows a mixed behavior between the resistor and the capacitor. ϕ and /Z/ values depend on the frequency, and the Nyquist plot has the shape of a semicircle. At low frequencies there is no dependency on the frequency. On the Bode plots, /Z/ value equals 1 kΩ and ϕ turns zero. On the Nyquist plot, the impedance only has a real component whose value is 1kΩ. Thus, at low frequencies only the resistor is contributing to the overall impedance.

Real systems often behave in a more complex way than ideal resistors and capacitors. For instance, measured resistances often change with frequency. Frequently, capacitors have a phase different from 90º. In this case, complex circuit elements like *constant phase elements (CPE)* provide a more real picture of the system.

In order to provide useful information, all the elements of an equivalent circuit must have a physical meaning. The circuit is built by taking into account all the parts of the system where the current flows. For instance, when a pair of electrodes is immersed in an electrolytic solution, current flows between them due to the mobility of the ionic species. Thus, the solution behaves as a resistor, whose resistance depends on the amount of ions present in the solution. Giving a physical meaning to the equivalent circuit is important because the same spectrum may be fitted with different equivalent circuits, thus rendering biased information. Ideally, it should be proved that every circuit element corresponds to the assigned physical magnitude. In the example above, how can we assure that the circuit element corresponds to the resistance of the solution? Experimentally, the ionic strength of the solution where the electrodes are immersed can be easily changed by adding a known amount of salt. Then, impedance spectra are obtained for each solution. If the circuit element associated to the resistance of the solution suffers the largest change, then its physical meaning is confirmed. It is noteworthy that, despite the effectiveness of this approach, the entire impedance spectrum changes upon perturbing the

system. In other words, the equivalent circuit represents a simplification of a more complex picture: the real system.

REFERENCES

1. Voet, D., Voet. J. G. *Biochemistry*, 2nd Ed., John Willey & Sons, 1995.

2. Berg, J. M., Tymoczko, J. L., Stryer, L. *Biochemistry*, 7th Ed., W. H. Freeman, 2007.

3. Alfred, N. *The antibody molecule*. Academic Press, 1975.

4. Eryl, L. *Antibody technology*. Oxford: Bios Scientific Publishers, 1995.

5. Chock, P. B. *et al*. *Enzyme dynamics and regulation*. Springer-Verlag, 1988.

6. Hermanson, T. J. *Bioconjugate techniques*. Academic. Elsevier, 1996.

7. Mosiello, L., Laconi, C., del Gallo, M. Development of a monoclonal antibody based potentiometric biosensor for terbuthylazine detection. *Sensors and Actuators B-Chemical,* **95,** 315-320, 2003.

8. Sekiguchi, T., Nakamura, M., Kato, M., *et al*. Immnunological Helicobacter pylori urease analyzer based on ion-selective field effect transistor. *Sensors and Actuators B-Chemical,* **67**, 265-269, 2000.

9. de la Rica R, Baldi A, Fernandez-Sanchez C. Local detection of enzymatic ion generation with polycrystalline silicon interdigitated electrodes and its application to biosensing. *Applied Physics Letters*, **90,** Art. No. 074102, 2007.

10. Hou, L. Y., Zhang, Z. J., Luo, L. R. Chemiluminescent imaging analysis of interferon alpha in serum samples *Analytical and Bioanalytical Chemistry*. **387,** 925-931, 2007.

11. Williams, E., Pividori, M. I,. Merkoci, A., *et al*. Rapid electrochemical genosensor assay using a streptavidin carbon-polymer biocomposite electrode. *Biosensors and bioelectronics*, **19,** 165-175, 2003.

12. Bloomfield, V. A., Crothers, D. M., Tinoco, I.. *Nucleic acids. Structures, properties and functions*. University Science Books, 2000.

13. Schena, M. *DNA microarrays: a practical approach*. Oxford University Press, 1999.

14. Skoog, D., Hallen, F. J., Nieman, T. A. *Principios de análisis instrumental*, 5ª Ed. McGraw Hill, 2001.

15. Sinclair, I. R. *Sensors and transducers. A guide*. Newnes, 1992.

16. Ristic, L. *Sensors technology and devices.* Artech House, 1993.

17.Eggins, B. R. *Chemical sensors and biosensors*. John Wiley & Sons, 2002.

18. Johnston, A., Thorpe, R. *Immunochemistry in practice*. Blackwell Science, 1996.

19. Gao, H., Guinchard, S., Crevoisier, F., *et al*. Microarrays and surface engineering for bioanalysis. *Chimia*, **57,** 651-654, 2003.

20 Fathman, C. G., Soares, L., Chan S. M., *et al*. An array of possibilities for the study of autoimmunity. *Nature*, **435,** 605-611, 2005.

21. Eisenberg, D., Marcotte, E. M., Xenarios, I., *et al*. Protein function in the post-genomic era. *Nature* **405,** 823-826, 2000.

22. Bild, A. H., Yao, G., Chang, J. T., *et al*. Oncogenic pathway signatures in human cancers as a guide to targeted therapies. *Nature* **439,** 353-357, 2006.

23. Bild, A. H., Potti, A., Nevins, J. R. Linking oncogenic pathways with therapeutic opportunities. *Nature reviews cancer* **6,** 735-U13, 2006.

24. Coppola, G., Geschwind D. H. Technology Insight: querying the genome with microarrays - progress and hope for neurological disease. *Nature clinical practice neurology*. **2,** 147-158, 2006.

25. Hoheisel, J. D. Microarray technology: beyond transcript profiling and genotype analysis. *Nature reviews genetics*. **7,** 200-210, 2006.

26 Green, N. S., Pass, K. A. Neonatal screening by DNA microarray: spots and chips. *Nature reviews genetics.* **6,** 147-151, 2005.

27. Lee, K. B., Park, S. J., Mirkin, C. A., *et al*. Protein nanoarrays generated by dip-pen nanolithography. Science **295,** 1702-1705, 2002.

28. Demers, L. M., Ginger, D. S., Park, S. J., *et al*. Direct patterning of modified oligonucleotides on metals and insulators by dip-pen nanolithography. *Science* **296,** 1836-1838, 2002

29. Bullen, D., Wang, X. F., Zou, J., *et al*. Design, fabrication, and characterization of thermally actuated probe arrays for dip pen nanolithography. *Journal of microelectromechanical systems*.**13,** 594-602, 2004.

30. Wang, X. F., Bullen, D. A., Zou, J., *et al*. Thermally actuated probe array for parallel dip-pen nanolithography. *Journal of vacuum science and technology-B.* **22,** 2563-2567, 2004.

31. Nam, J. M., Han, S. W., Lee, K. B., *et al*. Bioactive protein nanoarrays on nickel oxide surfaces formed by dip-pen nanolithography. *Angewandte chemie international edition*. **43,** 1246-1249, 2004

32. Lee, K. B., Lim, J. H., Mirkin, C. A. Protein nanostructures formed via direct-write dip-pen nanolithography. *Journal of the American Chemical Society*. **125,** 5588-5589, 2003.

33. Vega, R. A., Maspoch, D., Shen, C. K. F., *et al*. Functional antibody arrays through metal ion-affinity templates. *Chembiochem* **7,** 1653-1657, 2006.

34. Huff, J. L., Lynch, M. P., Nettikadan, S., *et al*. Label-free protein and pathogen detection using the atomic force microscope. *Journal of biomolecular screening* **9,** 491-497, 2004.

35. Lee, K. B., Kim, E. Y., Mirkin, C. A., *et al*. The use of nanoarrays for highly sensitive and selective detection of human immunodeficiency virus type 1 in plasma. *Nano Letters*, **4,** 1869-1872, 2004.

36. Dorey, A. P., Moore, J. H. *Advances in actuators*. IOP Publishing, 1995.

37. Singh, P., Aubry, N. Trapping force on a finite-sized particle in a dielectrophoretic cage. *Physical review E* **72,** Art. No. 016602, 2005.

38. Voldman, J., Toner, M., Gray, M. L., *et al*. Design and analysis of extruded quadrupolar dielectrophoretic traps. Journal of electrostatics **57,** 69-90, 2003

39. Gimsa, J., Eppmann, P., Pruger, B. Introducing phase analysis light scattering for dielectric characterization: Measurement of traveling-wave pumping. *Biophysiscal journal* **73,** 3309-3316, 1997.

40. Gadish, N., Voldman, J. High-throughput positive-dielectrophoretic bioparticle microconcentrator. *Analytical chemistry* **78,** 7870-7876, 2006.

41. Aldaeus, F., Lin, Y., Roeraade, J., *et al*. Superpositioned dielectrophoresis for enhanced trapping efficiency. *Electrophoresis* **26,** 4252-4259, 2005.

42. Li, H. B., Zheng ,Y. N., Akin, D., *et al*. Characterization and modeling of a microfluidic dielectrophoresis filter for biological species. *Journal of microelectromechanical systems*. **14,** 103-112, 2005.

43. Velev, O. D., Bhatt, K. H. On-chip micromanipulation and assembly of colloidal particles by electric fields. *Soft matter* **2,** 738-750, 2006.

44. Chen, D. F., Du, H., Li, W. H. A 3D paired microelectrode array for accumulation and separation of microparticles. *Journal of micromechanics and microengineering* **16,** 1162-1169, 2006.

45. Li, Y. L., Dalton, C., Crabtree, H. J., *et al*. Continuous dielectrophoretic cell separation microfluidic device. *Lab on a chip* **7,** 239-248, 2007.

46. Wang, Z. Y., Hansen, O., Petersen, P. K., *et al*. Dielectrophoresis microsystem with integrated flow cytometers for on-line monitoring of sorting efficiency. *Electrophoresis* **27,** 5081-5092, 2006.

47. Bown, M. R., Meinhart, C. D. AC electroosmotic flow in a DNA concentrator. *Microfluidics and nanofluidics* **2,** 513-523, 2006.

48. Tuukkanen, S., Toppari, J. J., Kuzyk, A., *et al*. Carbon nanotubes as electrodes for dielectrophoresis of DNA. *Nano Letters* **6,** 1339-1343, 2006.

49. Krupke, R., Linden, S., Rapp, M., *et al*. Thin films of metallic carbon nanotubes prepared by dielectrophoresis. *Advanced materials* **18,** 1468-1479, 2006.

50. Suehiro. J., Sano, N., Zhou, G. B., *et al*. Application of dielectrophoresis to fabrication of carbon nanohorn gas sensor. *Journal of electrostatics* **64,** 2006.

51. Zhang F. X., Srinivasan M. P. Self-assembled molecular films of aminosilanes and their immobilization capacities. *Langmuir* **20,** 2309-2314, 2004.

52. Lenigk, R., Carles, M., Ip, N. Y., *et al*. Surface characterization of a silicon-chip-based DNA microarray. *Langmuir* **17,** 2497-2501, 2001.

53. Onclin, S., Ravoo, B. J., Reinhoudt, D. N. Engineering silicon oxide surfaces using self-assembled monolayers. *Angewandte chemie-International edition* **44,** 6282-6304, 2005.

54. Barsoukov, E., MacDonald, J. R. *Impedance spectroscopy. Theory, experiment and applications*, 2nd Ed. John Wiley & Sons, 2005.
55. Bard, A. J., Faulkner, L. R. *Electrochemical methods. Fundamentals and applications*, 2nd Ed. John Wiley & Sons, 2001.

CONCLUDING REMARKS

In this work, the following goals were accomplished:

Interdigitated electrodes made of polycrystalline silicon were successfully fabricated and characterized. The electrodes had 3 μm width fingers separated by 3, 10 or 20 μm, respectively. An equivalent circuit for the electrodes immersed in a solution was proposed and tested. The feasibility and sensitivity of these devices for monitoring the resistivity and the dielectric properties of a solution using the proposed equivalent circuit was demonstrated. The resistivity of the solution was also successfully monitored by measuring the impedance at a fixed frequency.

The aforementioned electrodes were modified with the enzyme urease. They were able to detect local changes in resistivity due to the enzymatic conversion of urea to ionic species. Likewise, the suitability of this transduction system for the fabrication of immunosensors was demonstrated, using urease as a label of a model immunochemical reaction.

It was proved that polycrystalline silicon interdigitated electrodes were able to pre-concentrate and detect insulating microparticles. 3 μm diameter latex beads were accumulated onto the electrodes by positive dielectrophoresis. The presence of the particles was detected by monitoring either the conductivity or the dielectric properties of the solution. Variations in these parameters depended on the amount of beads present at the surface. These results show the feasibility of this approach for developing bead-based electrical biosensors.

Finally, patterns of 3-aminopropyltrimethoxysilane with the dimensions of carbon nanotubes were attained using a new concept in soft lithography. It was named gas transfer lithography. The morphological characteristics of the nanopatterns were investigated with an AFM. The positively charged amino-

modified areas were shown to selectively adsorb negatively charged oligonucleotides. This constituted a good example of the great potential of gas transfer lithography for chemical patterning of biomolecule nanoarrays.

I

Available online at www.sciencedirect.com
SCIENCE DIRECT®
Electrochemistry Communications 8 (2006) 1239–1244
electrochemistry communications
www.elsevier.com/locate/elecom

Polysilicon interdigitated electrodes as impedimetric sensors

Roberto de la Rica, César Fernández-Sánchez, Antonio Baldi *

Centro Nacional de Microelectrónica (IMB-CNM, CSIC), Campus UAB, 08193 Cerdanyola, Barcelono, Spain

Received 5 May 2006; received in revised form 29 May 2006; accepted 31 May 2006
Available online 7 July 2006

Abstract

The suitability of polysilicon as a material for the fabrication of interdigitated electrodes and their application to the development of sensors is studied in this work. The main interest in using this material lies in the possibility of obtaining integrated sensors with commercial CMOS technologies and simple post-processing steps. Electrodes with 3 μm finger width and 3, 10, and 20 μm spacing were fabricated and characterised. Conductivity measurements in the range from 4 to 50 μS/cm yielded a linear response with cell constants of 0.0416 cm^{-1}, 0.155 cm^{-1} and 0.33 cm^{-1}, respectively. Permittivity measurements in the range from $\varepsilon_r = 80.1$ to $\varepsilon_r = 1.89$ yielded a linear response and similar cell constants. The possibility to functionalise both the electrode fingers and the space in between them using a single silanisation process is an interesting advantage of polysilicon electrodes. An urease-based biosensor was obtained with this procedure and characterisation results are reported.

Keywords: Interdigitated electrodes; Polysilicon; Impedimetric sensor; Conductometric sensor; Biosensor

1. Introduction

Planar microelectrodes for impedimetric measurements offer many possibilities for the construction of physical, chemical and "bio-" sensors. Their robust and simple structure, their long term stability and reliability, and easy fabrication have attracted much attention from the sensor research community. Applications that have been proposed for these microelectrodes include measurement of the concentration of calcium [1], potassium [2], *p*(CO2) [3], pH [4], ethanol/methanol in gasoline [5], heavy metals [6], nitrate [7], urea [8,9], glucose [10], total prostate-specific antigen (PSA) [11], bacteria [12], red blood cells (hematocrit) [13], and detection of specific sequences of DNA [14]. In some applications, the measurement of a physical magnitude such as dielectric constant or conductivity of the media provides direct information of the analyte concentration [5,13]. In other applications, the deposition of a membrane or functional monolayer on top of the electrodes as a recognition element is necessary to obtain sensitivity and selectivity to particular species [1–4,6–14].

Different arrangements of electrodes (i.e. different number of electrodes and geometries) may be used for impedimetric measurements. Among them, interdigitated electrodes have significant advantages for certain applications: (1) their low cell constant (resistance to resistivity ratio) permit the measurement of very low conductivity solutions, (2) measurement of dielectric properties is possible thanks to a high inter-electrode capacitance (higher than stray capacitance even for conductive substrates), (3) the short penetration depth of electric fields make them less dependent on the measurement cell geometry and allow the use of thin membranes for tailoring selectivity.

In this paper, the suitability of polysilicon as a material for the fabrication of interdigitated electrodes and their application to the development of sensors is studied. Particularly, the feasibility of measuring solution conductivity and permittivity with polysilicon electrodes is demonstrated. The main interest in using this material lies in the possibility of fabricating the electrodes with commercial CMOS technologies and simple post-processing steps, and therefore being able to integrate them as sensors in a

* Corresponding author. Tel.: +34 935947700; fax: +34 935801496.
E-mail address: Antoni.baldi@cnm.es (A. Baldi).

1388-2481/$ - see front matter © 2006 Elsevier B.V. All rights reserved.
doi:10.1016/j.elecom.2006.05.028

more complex system-on-chip. Another interesting advantage is that this material can be easily modified following a one-step silanisation reaction. In this way, robust immobilisation of either biomolecules or membranes can be carried out on to both the electrode fingers and the area in between them with the aim of developing a sensor device. As an example, a fully functionalised biosensor for the detection of urea is also presented.

The basic structure of the interdigitated electrodes is depicted in Fig. 1. The polysilicon traces forming the interdigitated geometry are separated from the silicon substrate by a thick silicon dioxide layer. Fig. 2 shows the equivalent circuit of the interdigitated electrodes in aqueous solution. The elements that are repeated for each electrode have been grouped in a single equivalent component. This equivalent circuit is similar to the one previously proposed in [15]. The resistance and capacitance of the solution are represented by R_{sol} and C_{sol}. From these components, the resistivity ρ (or the conductivity σ) and the permittivity ε of the solution can be estimated, respectively. The ratio between measured components and actual physical parameters of the solution, the so-called cell constant, is defined as:

$$k \equiv R_{sol}/\rho = \varepsilon/C_{sol} \quad (1)$$

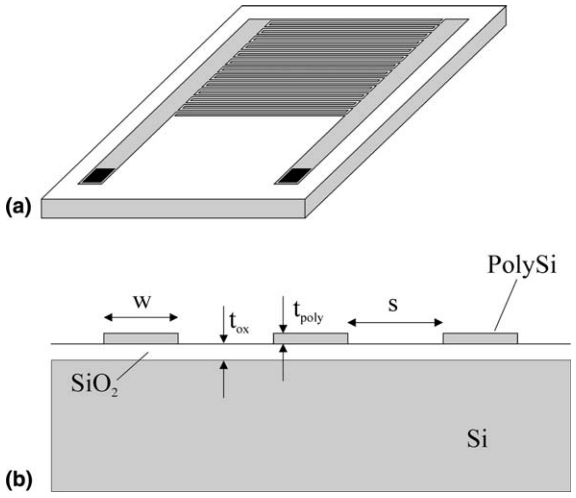

Fig. 1. Schematic representation of the interdigitated electrodes layout (a) and their cross-section (b). Geometrical parameters are indicated.

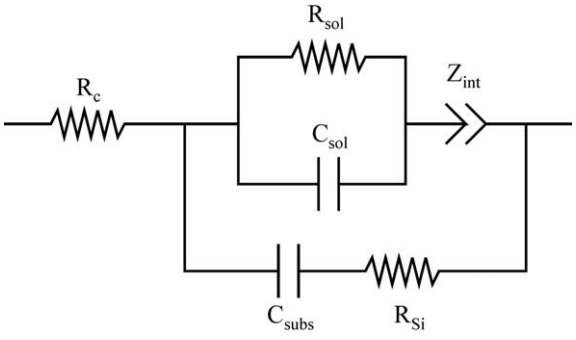

Fig. 2. Equivalent circuit of the interdigitated electrodes immersed in a solution.

The cell constant value is set by the electrode geometrical parameters. There are approximate analytical expressions to calculate the theoretical cell constant corresponding to a particular electrode geometry (defined by w and s parameters in Fig. 1b) [16]. However, for the present technology, where the thickness of the polysilicon fingers (t_{poly}) is not negligible compared to their width and spacing, the cell constant is more precisely calculated by finite element analysis (FEA) simulations. In the present work, the low frequency electromagnetic field simulation software Maxwell2D (Ansoft Inc.) has been used for this aim.

The resistance of the polysilicon traces is represented by R_c in the equivalent circuit. Polysilicon is more resistive, even if doped to degeneration, than noble metals typically used for the fabrication of interdigitated electrodes. However, thicker polysilicon layers can be deposited and patterned with standard processes, which partially compensates for the higher resistivity. The capacitance of the electrodes to the substrate is represented by C_{subs}, and its value depends on the thickness of the silicon dioxide layer isolating the electrodes from the silicon substrate. R_c and C_{subs} limit the minimum resistivity and permittivity that can be measured and should be minimised in the design. The resistance in series with C_{subs}, R_{Si}, represents the resistance of the silicon substrate.

The impedance of the interface between the polysilicon and the solution is represented in the equivalent circuit by Z_{int}. For a typical metal electrode in the presence of an electroactive compound, the interface impedance is represented by a Randless circuit. This circuit is composed of the double layer capacitance in parallel with the impedance of the charge transfer processes, the so-called faradic impedance. In the case of polysilicon electrodes, the impedance of the native oxide layer has to be added in series. This layer spontaneously grows on top of the polysilicon structures in contact with air. The presence of the native silicon oxide passivates the electrode surface, thereby obstructing the charge transfer processes between the polysilicon and electroactive compounds present in the interface. As a consequence, these electrodes seem to be unsuitable for electrochemical impedance measurements and the possibility to use them for that purpose has not been further studied. In the equivalent circuit presented here the whole interface impedance has been modeled by a constant phase element:

$$Z_{int} = \frac{1}{C_{CPE}(j\omega)^{\alpha_{CPE}}} \quad (2)$$

With the aim of studying the appropriateness of the proposed equivalent circuit, three different interdigitated electrode designs have been tested in this work. Every design has the same sensor area but different spacing between fingers, and therefore different number of fingers. The finger width and length is 3 μm and 1600 μm, respectively. The spacing between fingers is 3, 10 and 20 μm, with a total of 218, 101 and 57 fingers for each layout. The solution resistance, R_{sol}, should increase with decreasing number of fingers, and therefore the cell constant should also increase.

2. Experimental

2.1. Electrode fabrication

Fabrication starts with the thermal oxidation of a silicon wafer to form a 1.5-μm thick silicon oxide layer. Next, a 0.48-μm thick polysilicon layer is deposited by LPCVD at 100 mTorr and 630 °C and using SiH_4 as precursor gas. The polysilicon is doped to degeneration with phosphor at 950 °C and atmospheric pressure using a liquid source of $POCl_3$. After removing in Buffered Oxide Etch (BOE) the thin layer of oxide grown during the doping step, the polysilicon layer is patterned with standard photolithography and reactive ion etching. Subsequently, interconnect pads are formed on top of the resulting polysilicon electrodes by deposition and patterning of a 0.5-μm thick aluminium layer. Finally, a passivation coating consisting of 3000 Å of silicon oxide and 7000 Å of silicon nitride is deposited and patterned. In this latter step, the passivation is removed from the pads and from the interdigitated area. BOE solution is used to etch the silicon oxide layer because of its high selectivity towards this material, which ensures that polysilicon fingers are left intact.

2.2. Materials and methods

Urease from Jack Beans, urea, glycine, (3-aminopropyl)trimethoxysilane (APTMS) and glutaraldehyde were purchased from Sigma–Aldrich (Spain). All other chemicals were of analytical grade. Deionised water (resistivity > 18 MΩ) was used throughout this work.

2.3. Impedance measurements

All the impedance spectra were taken in the range from 10 kHz to 1 MHz with a SI 1260 SOLARTRON Impedance Analyzer, at 0V DC potential and 10 mV AC peak-to-peak amplitude. The experiments were performed with electrodes of each geometry (3×3, 3×10, 3×20 nomenclature will be used to refer to electrodes with $w = 3$ and $s = 3$, 10, and 20 μm, respectively). Impedance spectra were fitted with the aid of the Zview2 software to the equivalent circuit shown in Fig. 2. The goodness of the fittings were evaluated from the square of the standard deviation between the original data and the calculated spectrum, the so-called χ^2 value.

2.4. Urea biosensor fabrication

3×20 electrodes were cleaned by immersing them in a stirred 2.5% KOH solution for 30 min. APTMS was gas-phase deposited onto the chip surface by keeping the sensor close to the silane in a sealed chamber previously purged with nitrogen. This protocol avoids the formation of a thick layer of APTMS onto the silicon oxide [17]. The electrodes were left to react with the silane overnight, then rinsed with water and dried under a nitrogen stream. Subsequently, urease was covalently attached to the sensor surface using glutaraldehyde as a linker between the silanised surface and the enzyme. Thus, the modified electrode was kept in a stirred 8% glutaraldehyde solution in PBS buffer pH 7 for 1 h. Then, it was rinsed with deionized water, dried, and dipped in a 10 mg/ml urease solution in PBS overnight.

3. Results and discussion

3.1. Conductivity measurements

Solutions with different conductivities in the range from 4 μS/cm to 50 μS/cm were prepared by diluting a concentrated KCl solution and measuring the final conductivity with a CRISON μCM 2202 Conductimeter. The impedance spectra of a 3×20 sensor immersed in these solutions are shown in Fig. 3. Solutions with a lower conductivity have a larger semicircle (higher R_{sol}). It can be seen that a good agreement between real and fitted spectra was achieved (all the fittings had a χ^2 lower than 10^{-4}), thus validating the proposed equivalent circuit.

A comparison of the three assayed geometries for an 11.3 μS/cm KCl solution can be seen in Fig. 4. 3×20 electrodes show higher R_{sol} than 3×10 electrodes and 3×10 electrodes higher R_{sol} than 3×3 electrodes. This indicates that the 3×20 electrodes have a smaller cell constant than 3×10 and 3×3 ones, as was expected from the fact that each geometry has a lesser amount of fingers. Table 1 summarises the values for the different equivalent circuit elements and different geometries at this particular conductivity. The theoretical values obtained from FEA simulations for R_{sol} and C_{sol} are also included and show a reasonably good agreement with the experimental ones.

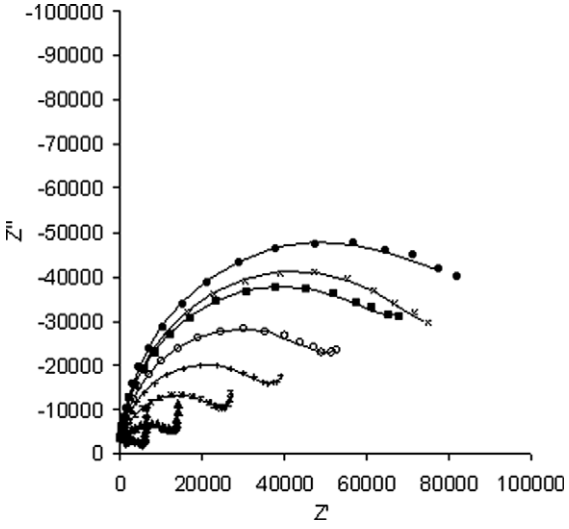

Fig. 3. Nyquist plot of 3×20 electrodes immersed in KCl solutions of different conductivity (56.4 μS/cm diamonds, 20.0 μS/cm triangles, 15.0 μS/cm stars, 8.50 μS/cm crosses, 6.58 μS/cm circles, 5.05 μS/cm squares, 4.37 μS/cm crosses, and 4.08 μS/cm diamonds). Dotted plots are the empiric impedance spectra; solid lines correspond to the fittings.

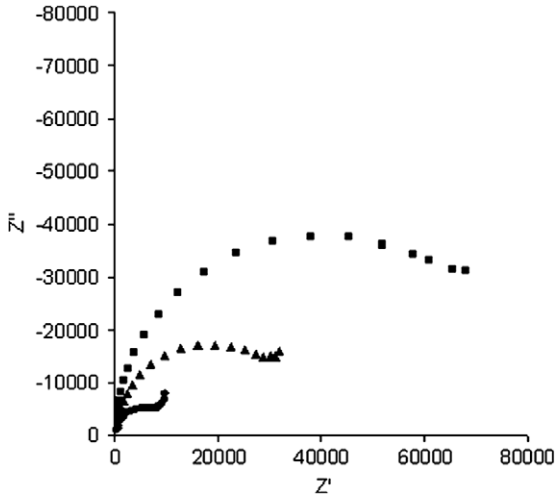

Fig. 4. Nyquist plot for 3×3 (circles), 3×10 (triangles) and 3×20 (squares) electrodes immersed in a KCl solution of conductivity 11.3 μS/cm.

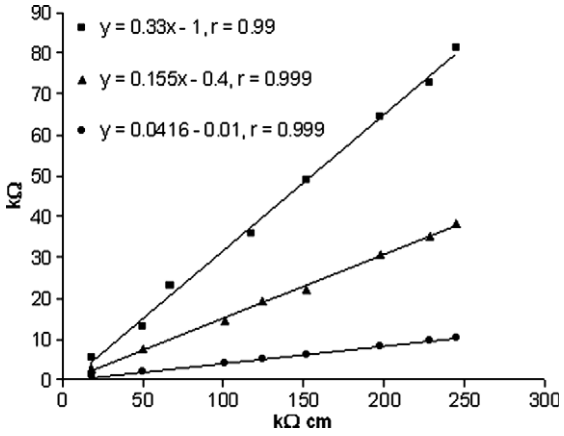

Fig. 5. Resistivity versus solution resistance plot for the three geometries assayed (3×3 circles, 3×10 triangles, 3×20 squares).

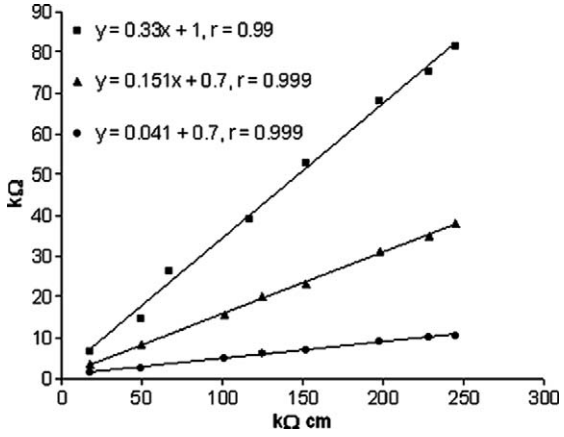

Fig. 6. Resistivity versus Z' at a fixed frequency for the three geometries assayed (3×3 circles, 3×10 triangles, 3×20 squares). The frequencies were 10 kHz for 3×20, 12.8 kHz for 3×10 and 2.5 kHz for 3×3.

The difference of about 10 pF between measurement and simulation values of C_{sol} is probably associated to a parasitic capacitance not taken in account in the simulations.

R_{sol} values for the different conductivities assayed were also obtained from the fitting and plotted versus the inverse of the conductivity (resistivity). A linear relationship was obtained. The slope of these curves is the electrodes cell constant. Results for each geometry are shown in Fig. 5. The cell constants of the 3×20, 3×10 and 3×3 electrodes and their 95% confidence interval are $0.33 \pm 0.02\ cm^{-1}$, $0.151 \pm 0.007\ cm^{-1}$ and $0.0407 \pm 0.0009\ cm^{-1}$, respectively. Alternatively, the real part of the measured impedance at a fixed frequency (Z') was plotted versus resistivity. This frequency was chosen to be at the local minimum of the Nyquist plot (between the semicircle and the low frequency tail), were the real part of the impedance approximates to R_{sol}. Results are shown in Fig. 6, with Z' measured at 10 kHz for the 3×20 electrodes, 12.6 kHz for 3×10 and 20 kHz for 3×3. A linear relationship between Z' and the resistivity can be observed. It is also important to note that the cell constant obtained with this methodology is the same as the one obtained from fitting the whole curve.

3.2. Permittivity measurements

In order to prove that the polysilicon interdigitated electrodes are suitable for the detection of changes in the permittivity of the medium, impedance spectra were taken in different solvents as well as in air. The assayed solvents were water ($\varepsilon_r = 80.1$), acetonitrile ($\varepsilon_r = 36.6$), ethanol ($\varepsilon_r = 25.3$), tetrahydrofuran ($\varepsilon_r = 7.52$) and hexane ($\varepsilon_r = 1.89$). Fitted plots were obtained as above. Bode plots for the real and fitted spectra of 3×3 electrodes are shown in Fig. 7. C_{sol} versus ε_r plots for all geometries are shown in Fig. 8, where a linear relationship can be observed. The slopes of the calibration curves (and their 95% confidence intervals) were 2.4 ± 0.2, 0.61 ± 0.02, and 0.303 ± 0.009 pF for the 3×20, 3×10 and 3×3 electrode geometries, respectively. The cell constants obtained from these values were 0.29, 0.14 and $0.037\ cm^{-1}$. Good agreement was observed with cell constant obtained from resistive measurements.

Table 1
Summary of equivalent circuit element values obtained from fitting of the experimental curves and from FEA simulations for 11.3 μS/cm

Geometry	R_{sol} measured (Ω)	R_{sol} simulated (Ω)	C_{sol} measured (pF)	C_{sol} simulated (pF)	R_{Si} (Ω)	R_c (Ω)	C_{subs} (pF)	C_{CPE} (nF)	α_{CPE}
3×3	3682	3918	180	163	60	267	32	9.5	0.88
3×10	13718	14598	51	44.3	150	256	26	5.8	0.88
3×20	29205	33496	27	19.7	250	197	23	23	0.73

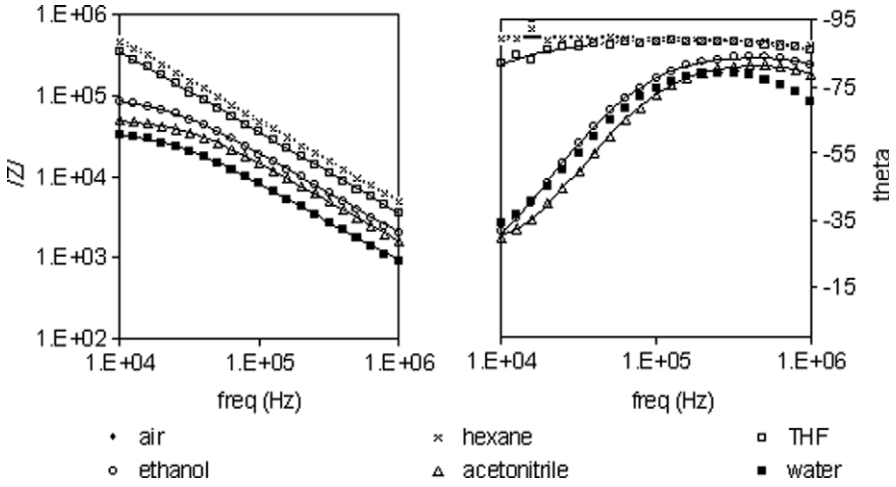

Fig. 7. Bode plots of 3×3 electrodes immersed in solvents with different permittivity. Dotted plots are the empiric impedance spectra; solid lines correspond to the fittings.

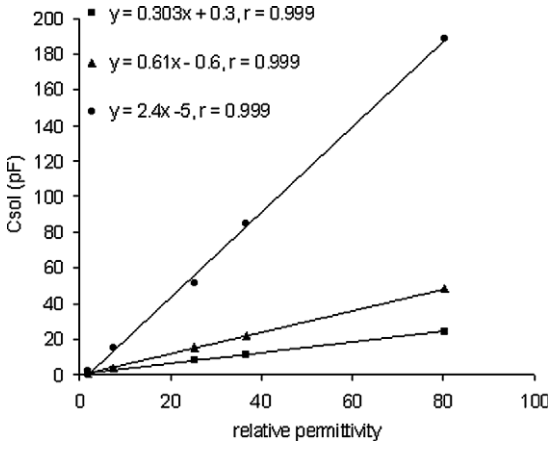

Fig. 8. Permittivity versus C_{sol} for the three geometries assayed (3×3 circles, 3×10 triangles, 3×20 squares).

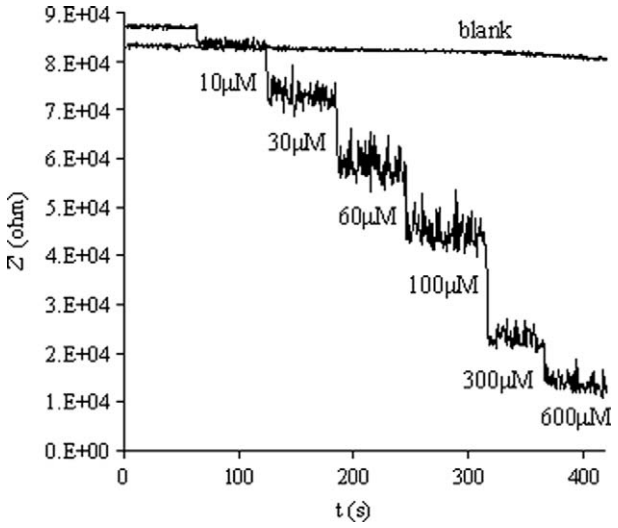

Fig. 9. Changes in Z' versus time upon the addition of urea for plain electrodes and urease-modified electrodes (3×20 electrodes).

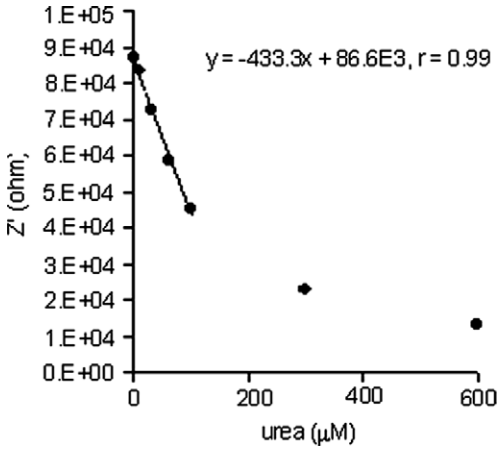

Fig. 10. Urea concentration versus Z' plot for the proposed biosensor.

3.3. Urea enzymatic sensor

The capability of the fabricated biosensor to detect changes in the concentration of urea was assayed. The sensor was immersed in a stirred 50 mM glycine solution pH 5.7 (conductivity 3.7 μS/cm) and the impedance measured at a set frequency of 10 kHz. The reaction catalysed by urease is described elsewhere [18]. In brief, the hydrolysis of urea causes the appearance of ammonium, bicarbonate and hydroxyl ions, therefore increasing the conductivity of the solution. The sensor response to the urea concentration was tested by adding the right amount of a 0.1 M urea stock solution every 60 s. Plain 3×20 electrodes were used as a blank. Results of the changes in Z' with time are depicted in Fig. 9. The relationship between Z' and the urea concentration was found to be linear in the range from 10 μM to 100 μM, with sensitivity of −433.3 Ω/μM (Fig. 10).

4. Conclusions

Polysilicon interdigitated electrodes with different geometries were fabricated and characterised. In particular, the

suitability of these electrodes to measure both the conductivity and permittivity of low ionic strength solutions was demonstrated. Linear responses were obtained in both cases and the cell constants showed good agreement with the theoretical ones obtained from simulations. In the case of conductivity measurements, it was also proved that measuring the real part of the impedance at an appropriate frequency also yielded a linear response, no further treatment of data being necessary to obtain this parameter. This feature is of particular interest when developing sensors devoted to real-time measurements, i.e. in flow systems.

Finally, an application of the proposed electrode arrangement to the fabrication of a conductometric urea biosensor was developed. It was proved that an urease-based sensor can be fabricated by covalently attaching the enzyme to the previously silanised sensor surface. The measurement of the impedance at a fixed frequency enabled the real-time monitoring of urea concentration.

Acknowledgements

Funding for this project was provided by the Ministry of Education and Science of the Spanish Government (Ref. TEC2004-00068/MIC), and the Consejo Superior de Investigaciones Científicas (CSIC) (Ref. 200560F0142).

References

[1] U. Trebbe, M. Niggemann, K. Cammann, G.C. Fiaccabrino, M. Koudelka-Hep, S. Dzyadevich, O. Shulga, J. Fresenius, Anal. Chem. 371 (2001) 734.
[2] A.E. Shvarev, D.A. Rantsan, K.N. Mikhelson, Sensor. Actuator. B 76 (2001) 500.
[3] A.R. Varlan, W. Sansen, Sensor. Actuator. B 44 (1997) 309.
[4] N.F. Sheppard Jr., M.J. Lesho, P. McNally, A.S. Francomacaro, Sensor. Actuator. B 28 (1995) 95.
[5] T. Hofmann, F. Bcckmann, S. Michaelis, J. Zacheja, J. Binder, S. Tagliante, Sensor. Actuator. A 61 (1997) 319.
[6] C. Chouteau, S. Dzyadevych, C. Durrieu, J.M. Chovelon, Biosens. Bioelectron. 21 (2005) 273.
[7] X. Wang, S.V. Dzyadevych, J.M. Chovelon, N. Jaffrezic-Renault, L. Chen, S. Xia, J. Zhao, Electrochem. Commun. 8 (2006) 201.
[8] P. Jacobs, J. Suls, W. Sansen, Sensor. Actuator. B 20 (1994) 193.
[9] A. Steinschaden, D. Adamovic, G. Jobst, R. Glatz, G. Urban, Sensor. Actuator. B 44 (1997) 365.
[10] S.V. Dzyadevicha, V.N. Arkhipova, A.P. Soldatkina, A.V. El'skaya, A.A. Shul'ga, Anal. Chim. Acta 374 (1998) 11.
[11] C. Fernandez-Sanchez, C.J. McNeil, K. Rawson, O. Nilsson, Anal. Chem. 76 (2004) 5649.
[12] N. Kordas, Y. Manoli, W. Mokwa, M. Rospert, Sensor. Actuator. B 43 (1994) 31.
[13] A.R. Varlan, P. Jacobs, W. Sansen, Sensor. Actuator. B 34 (1996) 258.
[14] L. Moreno-Hagelsieb, P.E. Lobert, R. Pampin, D. Bourgeois, J. Remacle, D. Flandre, Sensor. Actuator. B 98 (2004) 269.
[15] P. Van Gerwen, W. Laureyn, W. Laureys, G. Huyberechts, M. Op De Beeck, K. Baert, J. Suls, W. Sansen, P. Jacobs, L. Hermans, R. Mertens, Sensor. Actuator. B 49 (1998) 73.
[16] W. Olthuis, W. Streekstra, P. Bergveld, Sensor. Actuator. B 24–25 (1995) 252.
[17] Janildo L. Magalhaes, Leonardo M. Moreira, Ubirajara P. Rodrigues-Filho, Martha J. Giz, Marcelo A. Pereira-da-Silva, Richard Landers, Rita C.G. Vinhas, Pedro A.P. Nascente, Surf. Interf. Anal. 33 (2002) 293.
[18] W.Y. Lee, K.S. Lee, T.H. Kim, M.C. Shin, J.K. Park, Electroanalysis 12 (2000) 78.

II

Local detection of enzymatic ion generation with polycrystalline silicon interdigitated electrodes and its application to biosensing

Roberto de la Rica,[a] Antonio Baldi, and César Fernández-Sánchez
Centro Nacional de Microelectrónica (IMB-CNM, CSIC), Esfera UAB, Campus UAB, 08193 Cerdanyola del Vallés, Barcelona, Spain

(Received 28 December 2006; accepted 12 January 2007; published online 12 February 2007)

Chips containing polycrystalline silicon interdigitated electrodes are modified with the enzyme urease. The sensors are able to detect changes in the resitivity of the solution near their surface, where the enzymatic reaction generates charged species. The electrodes are also grafted with an antigen and queried with different amounts of urease labeled antibody. The response of the modified electrodes is proportional to the amount of enzyme attached to the surface by the biorecognition event, thus validating the assay for biosensing applications. © *2007 American Institute of Physics*. [DOI: 10.1063/1.2472718]

Patient-tailored prognosis, diagnosis, and therapy design are becoming achievable objectives due to the recent advances in genomics and proteomics. The chance of monitoring the state of a tissue, from detection of mutations in genomic deoxyribonucleic acid (DNA) to quantification of expressed ribonucleic acid levels and finding of proteins with an altered function, has opened a promising horizon in clinical biochemistry. Among the different approaches for biomolecule determination, biosensors offer the advantages of being robust, easy to handle, and capable of rendering information faster than other methodologies, which can only be performed in a laboratory by skilled staff. The signal generated by specific DNA-DNA or antigen-antibody interactions can be divided mainly in two groups. On the one hand, it may appear merely because of the presence of the analyte at the transducer surface. Examples of these so-called label-free biosensors are the detection of proteins by surface plasmon resonance,[1,2] quarz crystal microbalance,[3,4] or microcantilevers.[5] On the other hand, the signal may be triggered by the presence of a label, usually conjugated to another biomolecule, e.g., a labeled antibody that recognizes its antigen attached to the sensor surface. Enzymes are one of the most commonly used labels in biosensing. They can be easily conjugated to biomolecules via different cross linkers and well known chemical procedures, and the reactions they catalyze can be detected either optically[6,7] or electrochemically.[8–11]

In this letter, a biosensing principle is presented and tested. It consists in the generation of ions by an enzyme and the local detection of them by polycrystalline silicon interdigitated electrodes. The enzyme under study is urease, immobilized either via covalent linkage or by a biorecognition event at the transducer surface. In acidic media, the reaction catalyzed by urease can be described as

$$\begin{array}{lll} & \mathrm{O} & \\ & \| & \\ & \mathrm{C} & \overset{\text{urease}}{+ 3\mathrm{H_2O} \rightarrow \mathrm{CO_2} + 2\mathrm{NH_4^+} + 2\mathrm{OH^-}} \cdot \\ / & & \backslash \\ \mathrm{H_2N} & & \mathrm{NH_2} \end{array}$$

As a consequence, charged species appear at the electrodes surface. When the sensor is working under agitation, a stagnant layer a few micrometers thick is formed, where the arrival of substrate as well as the formation of products rapidly reaches a steady state. Thus, a concentration gradient of ions is created from the sensor surface to the bulk of the solution (Fig. 1). A suitable transducer, able to detect resistivity changes occurring close to its surface, should be very sensitive to the variations in the ion concentration created by the enzymatic reaction. Conversely, electrodes monitoring the resitivity of the bulk of the solution would measure a

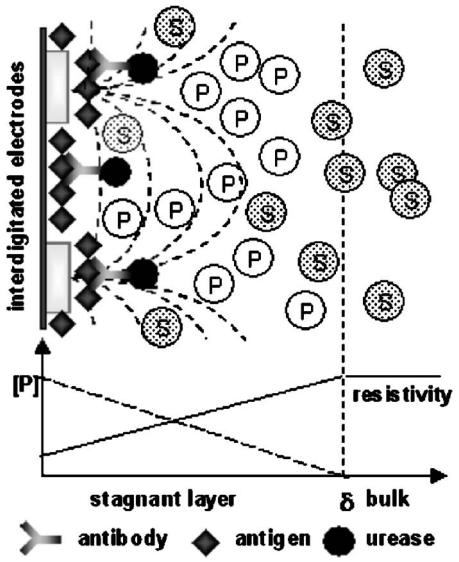

FIG. 1. Schematic representation of the bioassay. The biorecognition event drives urease to the electrodes surface, where the enzymatic reaction provokes the apparition of an ion concentration gradient. The geometry of the electrodes allows the local detection of the resultant resitivity change.

[a]Electronic mail: roberto.delarica@cnm.es

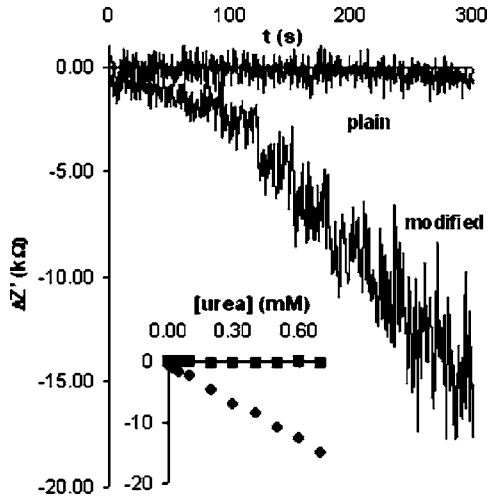

FIG. 2. Z' vs time plots for a plain and an urease modified sensor. Urea was added every 30 s. The inset shows the variation of Z' with the substrate concentration for the same data set.

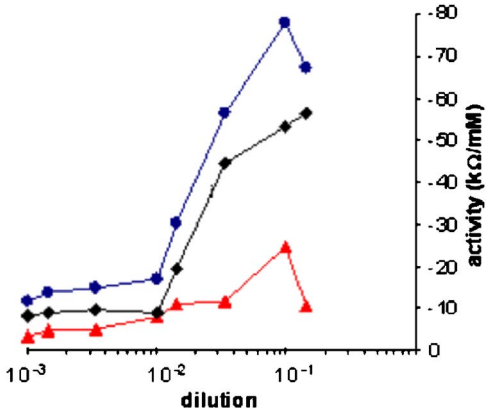

FIG. 3. (Color online) Subtraction of the response of antigen-grafted electrodes (circles) from the blank (triangle) yields an specific response curve (squares). The plot shows a correlation between the amount of urease attached to the surface (dilution) and the response of the electrode to urea.

much lower change because in this region the concentration of added ions is minimum.

Here, planar interdigitated electrodes with 3 μm width fingers are used as transducers. Recently, the capability of these electrodes to continuously monitor the resistivity of a solution by measuring the real part of the impedance at a given frequency was reported.[12] They are made of heavily doped polycrystalline silicon, which is an excellent platform for biomolecule grafting through silanization. The short penetration depth of the electric fields makes them more sensitive to changes occurring in the region extending a few micrometers from their surface to the bulk of the solution.[13] The capability of these electrodes to measure a resitivity decrease due to ion generation at their surface is evaluated with urease modified electrodes. Once cleaned with HF and 2.5% KOH, a chip was silanized with (3-aminopropyl)trimethoxysilane by putting it in a nitrogen purged chamber containing the silane overnight. The amino groups on the surface were turned to aldehyde ones by 1 h modification in a 12% glutaraldehyde solution in 0.1*M* carbonate buffer. The modified electrodes were dipped in a 1 mg/ml urease solution containing 50 mM sodium cyanoborohydride at 4 °C overnight. After a cleaning step in a 0.1% Tween 20 solution, the treatment rendered the sensor modified with covalently attached urease at its surface. Three experiments were then performed. In the first experiment the biosensor was immersed in a 50 mM glycine solution *p*H of 5.7, and the formation of charged species at its surface was monitored by measuring the real part of the impedance (Z') while adding the substrate at fixed time intervals (30 s). In the second experiment, two pairs of electrodes were placed in the reaction chamber, one of them was modified with urease and the other one was not. The electrodes recording the impedance were the plain ones, while the enzyme electrodes only contribute charged species to the bulk of the solution due to the catalytic reaction taking place at their surface. In this case, the ion generation is detached from the detection device and the monitored resistivity changes take place in the bulk of the solution. Finally, the experiment was repeated with a plain sensor alone, in order to monitor other variations not due to the enzymatic reaction. Results from this experiment were subtracted from the two former ones. Figure 2 shows the raw data of Z' versus time curve for the biosensor and the plain sensor. When the enzymatic reaction takes place at the electrodes, the resulting ion generation is detected and the relationship between the impedance and the urea concentration is linear in a certain range. Conversely, when the reaction takes place in the bulk of the solution, no impedance change is observed. This experiment undoubtedly demonstrates that the interdigitated electrodes used in these experiments are able to locally monitor the enzymatic production of charged species, and that this mode of detection is more sensitive to ion generation than bulk detection. Moreover, these biosensors are virtually independent of the chamber volume where the enzymatic reaction takes place, and therefore could be easily integrated in a microfluidic device.

Once the transduction principle is demonstrated, the feasibility of the proposed assay for biosensing is tested. The reaction between rabbit IgG (antigen) and urease labeled anti rabbit IgG (antibody) is used as the biorecognition event. The conjugation of the enzyme to the antibody has been reported elsewhere.[14] Rabbit IgG was grafted to the chip surface as before. The sensors were blocked in 100 mM tris(hydroxymethyl)aminomethane (TRIS) buffer, *p*H of 8.6 containing 1% albumin from bovine serum, and 50 mM ethanolamine at 4 °C overnight. Dilutions from 1:7 to $1:10^3$ of urease labeled antibody were prepared in 100 mM TRIS buffer *p*H of 7 containing 10 mM thioacetamide, 10 mM Ethylenediaminetetraacetic acid, and 140 mM NaCl. Antigen modified electrodes were dipped for 1 h in these solutions and, as a result of the biorecognition event, the electrodes were coated with different amounts of enzyme. Upon cleaning in 0.1% Tween 20, the biosensors were calibrated with urea as decribed above, and the slope of the linear part of the curve Z' versus concentration taken as a measure of the activity of the enzyme electrode. A blank curve was also obtained by interrogating anti rabbit IgG grafted electrodes with urease labeled anti rabbit IgG. Subtraction of the antigen curve to the blank curve rendered the plot corresponding to the specific interaction. When the activity is plotted versus the antibody dilution in semilogarithmic scale, a typical sigmoidal curve with a linear range is obtained (Fig. 3). These experiments confirm that the proposed biosensing principle can be applied to detect and quantify proteins. These results, together with the ones shown above, and the fact that the electrodes are miniaturized and made with well known pro-

cesses in the microelectronics industry, make the biosensors good candidates for the fabrication of integrated protein arrays.

[1]R. Kurita, Y. Yokota, Y. Sato, F. Mizutani, and O. Niwa, Anal. Chem. **78**, 5525 (2006).
[2]N. Kanoh, M. Kyo, K. Inamori, A. Ando, A. Asami, A. Nakao, and H. Osada, Anal. Chem. **78**, 2226 (2006).
[3]A. E. Gerdon, D. W. Wright, and D. E. Cliffel, Anal. Chem. **77**, 304 (2005).
[4]H. Zeng, H. Wang, F. Chen, H. Xin, G. Wang, L. Xiao, K. Song, D. Wu, Q. He, and G. Shen, Anal. Biochem. **351**, 69 (2006).
[5]G. Wu, R. H. Datar, K. M. Hansen, T. Thundat, R. J. Cote, and A. Majumdar, Nat. Biotechnol. **19**, 856 (2001).
[6]T. Konry, A. Novoa, Y. Shemer-Avni, N. Hanuka, S. Cosnier, A. Lepellec, and R.S. Marks, Talanta **77**, 1771 (2005).
[7]W. L. Xing, L. R. Ma, Z. H. Jiang, F. H. Cao, and M. H. Jia, Talanta **52**, 879 (2000).
[8]J. Albers, T. Grinwald, E. Nebling, G. Piechotta, and R. Hintsche, Anal. Bioanal. Chem. **377**, 521 (2003).
[9]C. Fernández-Sánchez, M. B. González-García, and A. Costa-García, Biosens. Bioelectron. **14**, 917 (2000).
[10]M. S. Wilson and W. Nie, Anal. Chem. **78**, 6476 (2006).
[11]C. Fernández-Sánchez, C. J. McNeil, K. Rawson, and O. Nilsson, Anal. Chem. **76**, 5649 (2004).
[12]R. de la Rica, C. Fernández-Sánchez, and A. Baldi, Electrochem. Commun. **8**, 1239 (2006).
[13]N. F. Sheppard, D. J. Mears, and A. Guiseppi-Elie, Biosens. Bioelectron. **11**, 967 (1996).
[14]T. J. Hermanson,*Bioconjugate Techniques* (Academic, Elsevier, 1996), p. 173.

III

Electric preconcentration and detection of latex beads with interdigitated electrodes

Roberto de la Rica,[a] César Fernández-Sánchez, and Antonio Baldi
Centro Nacional de Microelectrónica (IMB-CNM, CSIC), Esfera UAB, Campus UAB, 08193 Cerdanyola del Vallés, Barcelona, Spain

(Received 7 March 2007; accepted 24 March 2007; published online 23 April 2007)

Latex beads are adhered to the surface of a chip containing polycrystalline silicon interdigitated electrodes by positive dielectrophoresis. The presence of the microparticles induces a change in the distribution of the electric fields and currents that can be detected by measuring either the conductance or the capacitance at the electrode terminals. This combination of actuation and detection with a single device is proposed as a suitable system applicable to biosensing.
 [DOI: 10.1063/1.2731311]

Bead-based sensors are becoming common tools in bioanalytical chemistry. One of the most popular approaches uses paramagnetic particles as mobile substrates, where captured biomolecules are immobilized. A magnetic field is applied in order to attract the beads to the transducer surface. As a result of a biorecognition event, a signal, either electrochemical,[1] optical,[2] or magnetoresistive,[3,4] is generated. Magnetoresistive detection systems are gaining considerable interest in recent years.[5] The recognition between the capture element and the analyte results in the attachment of the beads to the sensor surface, where the presence of the magnetic particles is detected by a change in the resistivity of the material. Giant magnetoresistive devices,[6] anisotropic magnetic resistive rings,[7] Hall effect sensors,[8–10] as well as spin valves[11] and magnetic tunnel junction structures[12,13] have been proposed as suitable transducers for this kind of measurements.

In the present work, an alternative approach based on electric preconcentration and detection of latex beads is presented and tested. It consists in the accumulation and adsorption of the microparticles at the surface of a pair of interdigitated electrodes by positive dielectrophoresis, followed by their impedimetric detection. The electrodes are made of polycrystalline silicon. Their capability of measuring both the conductivity (σ) and the permittivity (ε) of the solution where they are immersed has been previously demonstrated.[14] The conductance (G) and the capacitance (C) measured at the electrodes are inversely proportional to these two magnitudes, respectively, by the cell constant (k):

$$C = \frac{\varepsilon}{k}, \tag{1}$$

$$G = \frac{\sigma}{k}. \tag{2}$$

The cell constant depends on both the geometry of the electrodes and the geometry of the space between the electrodes filled with the solution. The presence of insulating objects at the electrode surface alters the electric field distribution and the path of currents, thus changing the geometry of the cell (Fig. 1). This variation can be monitored by a change in the measured conductance or capacitance. The magnitude of the change in the cell constant depends on both the size of the insulating objects and their surface coverage. Translated to the system under study, beads with larger radius give rise to a larger signal as individuals, leading to a more sensitive detection, whereas smaller particles lead to a higher amount of beads per unit area, thus allowing a wider dynamic range.

Dielectrophoresis refers to the force on polarizable particles in a spatially nonuniform electric field and provides a suitable method for manipulating microparticles in liquid suspension. Two types of forces can be exerted: particles can be pulled towards points of maximum electric field (termed positive dielectrophoresis) or pushed towards locations of minimum electric field (termed negative dielectrophoresis). Here, positive dielectrophoresis is used in order to accumulate beads at the electrode fingers, where the electric field lines converge and the presence of the insulating microparticles has a greater impact on the cell constant (Fig. 2). Latex beads remain adhered to the surface after the dielectrophoretic force is turned off.[15] This dielectrophoretically driven adhesion of beads emulates microparticle attachment by a biorecognition event, like in magnetoresistive biosensors.[5] Interdigitated electrodes with 3 μm width fingers separated by 10 μm and 3 μm diameter latex beads are used in this work. Electrodes with similar electric field penetration depth have been previously used in dielectrophoretic accumulation of latex particles.[15,16]

In order to enhance the adhesion of beads, the sensors were grafted with 3-aminopropyltrymethoxysilane in a gas-phase procedure, by closing them in a previously nitrogen saturated chamber containing the silane, overnight. Hydrocarbonated chains in the silane render the surface more hydrophobic, promoting van der Waals interactions with the particles, and the terminal amino groups provide positive charges that can interact with negative counterparts present at the bead surface. Dielectrophoresis was performed after applying a drop of 0.25% (w/v) beads in 250 mM glycine buffer, which has a conductivity of 15 μS/cm. Amino-acid-based buffers have been previously used as low conductivity media in on-chip electrophoresis experiments[17,18] and protein detection biosensors.[19] A peak-to-peak potential of 1 V was applied, and the frequency was set at 5 kHz. Figure 3 shows images of the electrodes after different accumulation times.

[a]Electronic mail: roberto.delarica@cnm.es

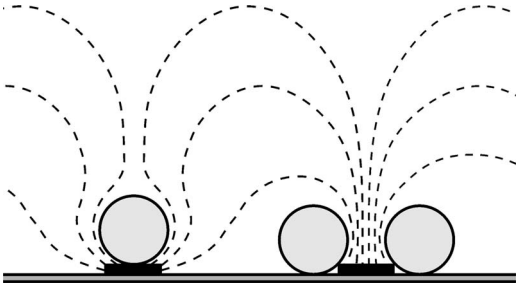

FIG. 1. Schematic representation of the detection system. Particles are attracted to the points of maximum electric field, changing the field lines distribution.

As expected, beads preferably adhere to the surface of the electrodes, either at the edges or on top. All the particles present in a certain area were counted in order to assess the on-chip bead density. These pictures clearly demonstrate that the proposed electrodes are able to concentrate micron-sized latex particles by positive dielectrophoresis.

Variation in the electrical properties of the cell caused by the presence of the microparticles was evaluated with the following experiment. An impedance spectrum of the bead-modified electrodes was taken from 1 MHz to 10 kHz applying a 10 mV amplitude excitation signal, in 250 mM glycine buffer, after each accumulation step. The spectra were fitted to an equivalent circuit in order to obtain the resistance and the capacitance of the solution. Details about the fitting procedure have been published elsewhere.[14] Resistance values were converted to conductance ones by simply inverting them. Results were translated into percentages, taking the plain sensor without beads as a reference. A parallel blank experiment was also performed by repeating the dielectrophoresis with another sensor in a solution containing no beads. These measurements monitor changes in the magnitudes of interest due to other factors, such as temperature drift or carbon dioxide diffusion, and were subtracted from the former ones. Figure 4 shows a plot of the variation in conductance and capacitance versus bead density. Saturation at high bead density values is caused by accumulation in the space between the fingers, where the impact of the insulating particles in the geometry of the cell is lower than that at the electrode surface. Both capacitance and conductance measurements give rise to comparable plots, as expected from a change in the cell constant, with a 2×10^3 bead^{-1} mm^2 slope

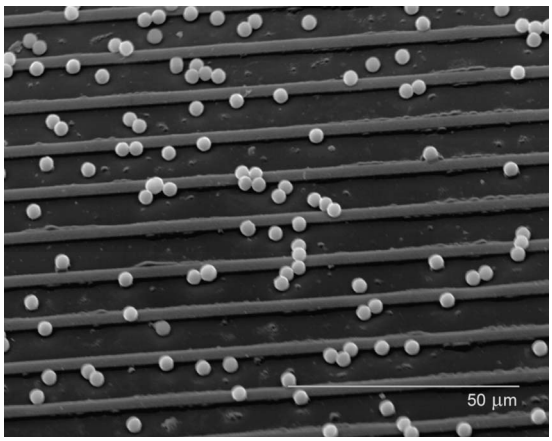

FIG. 2. Scanning electron microscopy image of the 3 μm width beads adhered at the sensor surface.

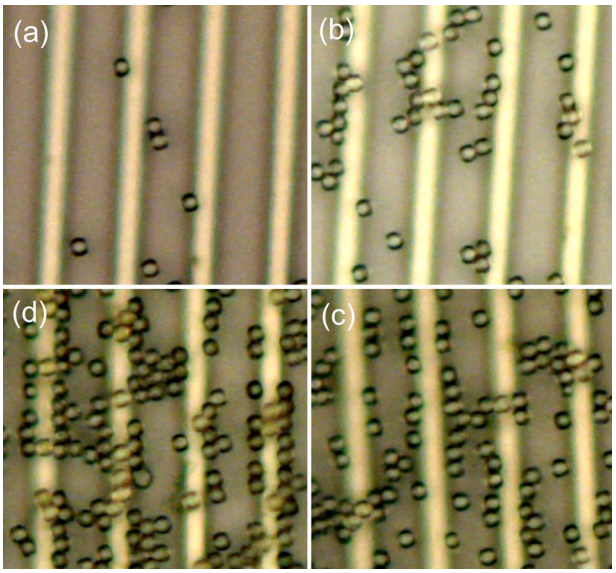

FIG. 3. Images of bead-coated electrodes with (a) 0.2, (b) 2, (c) 3, and (d) 8×10^3 mm^{-2} bead density.

in the linear part of the curve. These experiments prove that 3 μm diameter insulating microparticles can be detected using interdigitated electrodes with the proposed geometry.

In conclusion, a bead-based electric actuation and transduction system has been presented and tested. This approach is comparable to magnetoresistive biodetection, that is, dielectrophoretic accumulation substitutes magnetic preconcentration and impedimetric transduction replaces magnetoresistive detection. Polycrystalline silicon interdigitated electrodes can be fabricated with complementary metal-oxide-semiconductor technologies and modified with biomolecules, i.e., antibodies.[19] Latex beads modified with a wide variety of capture biomolecules are commercially available. Thereby, a biosensor may be easily developed, the analyte acting as a bridge between the transducer surface and the dielectrophoretically preconcentrated beads. Combination of these electrodes with microfluidics for bead manipulation

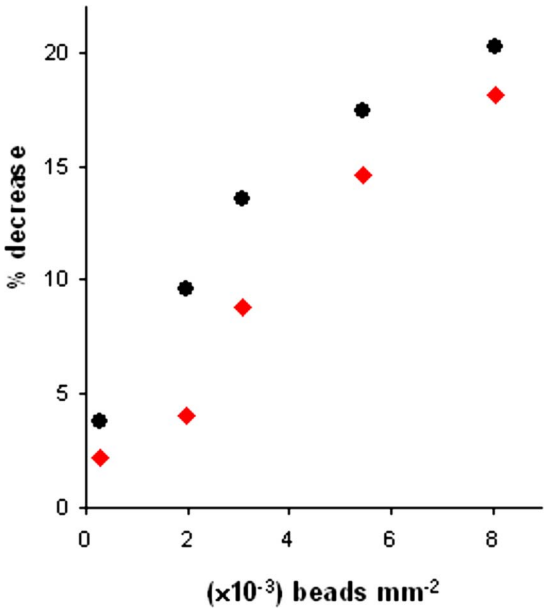

FIG. 4. (Color online) Percentage decrease in the conductance (circles) and the capacitance (squares) of the solution for different bead coverages.

makes the proposed detection system an appealing alternative for fully integrated biosensors and laboratory-on-chip systems.

Two of the authors (C.F.-F. and A.B.) acknowledge the Spanish Ministry of Science and Education for the award of a Ramón y Cajal contract.

[1]V. N. Goral, N. V. Zaytseva, and A. J. Baeumner, Lab Chip **6**, 414 (2006).
[2]S. Dubus, J. F. Gravel, B. Le Drogoff, P. Nobert, T. Veres, and D. Boudreau, Anal. Chem. **78**, 4457 (2006).
[3]M. Brzeska, M. Panhorst, P. B. Kamp, J. Schotter, G. Reiss, A. Pühler, A. Becker, and H. Brückl, J. Biotechnol. **112**, 25 (2004).
[4]G. Kurlyandskaya and V. Levit, Biosens. Bioelectron. **20**, 1611 (2005).
[5]D. L. Graham, H. A. Ferreira, and P. P. Freitas, Trends Biotechnol. **22**, 455 (2004).
[6]R. L. Edelstein, C. R. Tamanaha, P. E. Sheehan, M. M. Miller, D. R. Baselt, L. J. Whitman, and R. J. Colton, Biosens. Bioelectron. **14**, 805 (2000).
[7]M. M. Miller, G. A. Prinz, S.-F. Cheng, and S. Bounnak, Appl. Phys. Lett. **81**, 2211 (2002).
[8]P. A. Besse, G. Boero, M. Demierre, V. Pott, and R. Popovic, Appl. Phys. Lett. **80**, 4199 (2002).
[9]L. Ejsing, M. F. Hansen, and A. K. Menon, Appl. Phys. Lett. **84**, 4729 (2004).
[10]G. Mihajlović, P. Xiong, and S. von Molnár, Appl. Phys. Lett. **87**, 112502 (2005).
[11]L. Lagae, R. Wirix-Speetjens, J. Das, D. Graham, H. Ferreira, P. P. Freitas, G. Borghs, and J. De Boeck, J. Appl. Phys. **91**, 7445 (2002).
[12]W. F. Shen, X. Y. Liu, D. Mazumdar, and G. Xiao, Appl. Phys. Lett. **86**, 253901 (2005).
[13]S. G. Grancharov, H. Zeng, S. H. Sun, S. X. Wang, S. O'Brien, C. B. Murray, J. R. Kirtley, and G. A. Held, J. Phys. Chem. B **109**, 13030 (2005).
[14]R. de la Rica, C. Fernández-Sánchez, and A. Baldi, Electrochem. Commun. **8**, 1239 (2006).
[15]J. Auerswald, D. Widmer, N. F. De Rooij, A. Sigrist, T. Staubli, T. Stöckli, and H. F. Knapp, Electrophoresis **26**, 3697 (2005).
[16]N. Gadish and J. Voldman, Anal. Chem. **78**, 7870 (2006).
[17]C. F. Edman, D. E. Raymond, D. J. Wu, E. Tu, R. G. Sosnowski, W. F. Butler, M. Nerenberg, and M. J. Heller, Nucleic Acids Res. **25**, 4907 (1997).
[18]R. G. Sosnowski, E. Tu, W. F. Butler, J. P. O'Connell, and M. J. Heller, Proc. Natl. Acad. Sci. U.S.A. **94**, 1119 (1997).
[19]R. de la Rica, A. Baldi, and C. Fernández-Sánchez, Appl. Phys. Lett. **90**, 074102 (2007).

Annex

Chemically active nanopatterns with gas transfer lithography

Roberto de la Rica[1*], César Fernández-Sánchez[1], Ernest Mendoza[2], Andreu Llobera[1] & Antonio Baldi[1]

Departamento de Micro- y Nanosistemas, Instituto de Microelectrónica de Barcelona (IMB-CNM, CSIC), Campus UAB, 08193 Bellaterra, Barcelona, Spain.

Departament de Nanobiosensors i Nanobiofísica, Institut Català de Nanotecnologia, Campus UAB, 08193 Bellaterra, Barcelona, Spain

* e-mail: roberto.delarica@cnm.es

Soft lithography[1-3] comprises a family of surface patterning techniques based on the use of a polymeric impression of a relief substrate or master. In micro contact printing this negative replica is used as a stamp for printing molecules onto a receiving substrate[4]. Despite its appealing merits, this methodology is not well suited for replicating sub-10 nm sized features. Here, a new approach that overcomes this limitation is reported. We call this technique gas transfer lithography. Reactive amino-modified patterns with the dimensions of carbon nanotubes are obtained onto silicon substrates. The modified surfaces are intended as primary layers for "bottom-up" fabrication processes, for instance in biomolecule nanoarray[5] and nanowire[6] manufacture. The combination of this new approach with techniques like focused ion beam or electron beam lithography for the fabrication of masters opens a new horizon in mass scale production of nanoengineered substrates of interest for the biotechnology and semiconductor industry.

Figure 1 summarizes the replica process. The master was prepared by adsorbing carbon nanotubes on a silicon substrate. Carbon nanotubes have nanometer scale diameters and micrometer size lengths, and represent a paradigmatic model to test the potential of gas transfer lithography[7]. Poly(dimethylsiloxane) (PDMS) prepolymer is poured onto the master, where it adopts the shape of the nanotubes. After curing, the PDMS mould is peeled away and placed in a reaction chamber containing the molecules to be grafted. PDMS loads up with the volatile molecules due to its characteristic permeability to gases. The next step consists in placing the mould onto the receiving substrate, in this case an oxidized silicon

wafer. PDMS adhesion results in the formation of cavities with the shape of the original nanotubes, wherein gas phase molecules are transferred by diffusion and react with the exposed surface. After removing the mould, a surface patterned with the molecules of interest is obtained.

3-aminopropyltrimethoxysilane (APTMS) is the molecule selected to be patterned. The electrophilic silicon atom reacts with silanol groups present on the oxide surface to form stable siloxane bonds, whereas the nitrogen group in the amino residue has a strong nucleophilic nature, and is an excellent platform for subsequent chemical modification. Moreover, it provides positive charges that enhance the adhesion of negatively charged molecules and structures like DNA[8,9] and metallic colloids[10,11]. Regarding the substrate, silicon is a material of prime interest in the semiconductor industry. Furthermore, the present approach could be easily adapted to the deposition of other molecules from gas phase, for example alkanethiols on gold substrates[12].

The proposed procedure has some characteristics that make it more suitable than other soft lithographic techniques for downscaling molecule nanopatterning. First, molecule grafting occurs in a well delimited cavity, thus avoiding spreading of the reactive molecules outside the pattern. Second, unlike contact printing, the proposed methodology is not dependent on the application of a controlled pressure on the mould. Therefore, in gas transfer lithography pressure and contact time are not critical. As a consequence, the grafting process is inherently more reproducible and the resulting patterns fit better to the master

features. Third, the use of nanometre sized cavities instead of protruding features to define the pattern enables attaining individual widely spaced features. In this case, the area of the PDMS in contact with the receiving surface is large and the grafting step performs easily without mould deformation. Conversely, in techniques based on printing, the mould would probably collapse at the space between the patterns. Apart from these distinctive characteristics, gas transfer lithography shares the striking features of easy availability, high throughput and low cost with all the soft lithography approaches.

Atomic force microscope (AFM) was used to investigate the morphology of the patterned surfaces. Figure 2a shows an image of an original carbon nanotube present at the master. It appears as a bended worm-like structure onto the oxide surface. APTMS replica consists in regions with a slight increase in roughness and the shape of the original nanotubes (Fig. 2b). In order to further demonstrate the presence and reactivity of the amino-modified patterns, a site-specific DNA adsorption experiment was performed. The patterned surface was immersed in a solution containing a 12-mer oligonucleotide. The negative phosphate groups of DNA are attracted by the positive amino residues of the pattern, and as a result, the biomolecules preferably adsorb at the modified areas. The topographic changes induced by the presence of the biomolecule were investigated with the AFM (Fig 2c). The patterns appear now more contrasted, as expected from the increase in height caused by the presence of the oligonucleotides.

A more detailed analysis can be extracted from cross-sectional plots of the AFM images (Fig. 3). Multi-walled nanotubes appear as very wide, sprawled objects, though it is well known that they are cylindrical structures. This widening effect is due to convolution in the measurement, that is, the AFM tip width is added to the lateral dimensions of the pattern. As a consequence, the diameter of the nanotube is better estimated from the peak height, whose value is 8.5 nm.

The cross-sectional plot also provides valuable information about the success of the replica process. Background noise in the Z axis was calculated as the mean value of the peak heights at 150 points outside the pattern and subtracted in subsequent cross-sectional plots. Then, nine evenly distributed cross-sectional plots where obtained along the structures. A mean step of 0.5 ± 0.3 nm is obtained for the APTMS pattern (variability is expressed as the standard deviation). This result is consistent with the formation of a monolayer of APTMS molecules[13]. Silane molecules present reactive groups that are chemically complementary and often tend to form undesired oligomers. This phenomenon is more pronounced in APTMS layers due to the presence of the amino functionality, which can react with the silanol groups present in other APTMS molecules. Herein, AFM analysis suggests that gas transfer lithography is useful for obtaining high quality silane patterns.

The same data treatment was performed with the images corresponding to the site-specific DNA adsorption experiment. The mean step value increases to 1.5 ± 0.6 nm. The mean 1 nm height increase is in accordance with the attachment of

single-stranded DNA molecules. This result confirms both the presence and the reactivity of the amino-modified patterns onto the silicon substrate.

Finally, it is noteworthy that the cross-sectional plots have comparable lateral dimensions. Provided that the nanotubes have widths below 10 nm, these results demonstrate the feasibility of gas transfer lithography for sub-10 nm chemical patterning. These are the smallest silane replicas ever reported. Pattern size of photolithographically etched silane self-assembled monolayers is diffraction limited[14]. The accomplishment of sub-100 nm resolution is restricted to expensive lithography equipment used in advanced integrated circuit fabrication. Approaches based on inking and printing, like micro contact printing[6,15-16] and dip-pen nanolithography[17-20] enable sub-micrometer patterning, though in particular cases the sub-100 nm patterns have been achieved. The main problem of these approaches relies on the use of a wet process for grafting the silanes, which leads to formation of undesired polymers. Nanoimprint lithography yields patterns with similar resolution[21-22]. Better results have been achieved with electron beam lithography patterned PMMA layers and gas phase silane grafting of the resulting exposed areas. With this methodology, chemical functionalities down to the 20-25 nm feature size level were achieved[23]. However, it proved to be unsuitable for APTMS patterning, due to the creation of thick deposits attributable to gel formation. Silane patterns around 20 nm have also been reported for certain types of scanning probe lithography, like field-induced oxidation[24] (FIO) or scanning probe anodization[25]. Nevertheless, the use of direct writing approaches for mass scale fabrication is unaffordable. In conclusion, gas

transfer lithography combines a high resolution and high throughput with a low cost and simplicity, which makes this approach an appealing alternative for chemical nanopatterning.

Methods

Replica process

A solution of multi walled carbon nanotubes in dichlorobenzene was sonicated for 10 minutes and centrifuged at 14,000 rpm for 15 minutes, prior to use. 1 mL of the resulting supernatant was collected and spread onto a 4-inch silicon wafer with thermally grown oxide. After 1 hour, the wafer was rinsed with deionized water and dried in a stream of nitrogen. The prepolymer consisted in a 10:1 (v:v) mixture of PDMS-Sylgard Silicone Elastomer 184 and Sylgard Curing Agent 184 (Dow Corning Corp.). The mixture was put under vacuum to remove dissolved oxygen. After pouring on the master, it was cured at 80ºC for 30 minutes. The resulting PDMS moulds were kept in the reaction chamber containing 3-aminopropyltrimethoxysilane at room temperature overnight. Then, they were blown with nitrogen and placed onto the receiving substrate for 5 minutes. After mould removal, the substrates were rinsed with water and dried with nitrogen. The receiving substrates were 1.5 cm^2 dice of silicon (using the same type of wafers as above) cleaned in a 2.5% KOH solution.

Site-specific DNA adsorption

The nanopatterned substrates were immersed in a 100μM solution of a 12-mer oligonucleotide in deionized water. After 1 hour, they were rinsed with deionized water and dried with nitrogen.

AFM images acquisition

The experiments were performed with a Pico Plus Atomic Force Microscopy working in acoustic mode using high aspect ratio cantilevers. Images were processed with WSxM software.

Acknowledgements

We thank V. Cadarso for help.

Author contributions

R.R conceived the idea. C.F.S., A.B. and R.R designed and carried out the experiments, and wrote the article. A.L. helped in the moulding technique. E.M. and R.R. performed AFM imaging and analysis.

The authors declare that they have no competing financial interests.

1. Gates, B. D., *et al*. New approaches to nanofabrication: molding, printing and other techniques. *Chem. Rev*. **105,** 1171-1196 (2005).

2. Xia, Y. & Whitesides, G. M.. Soft Lithography. *Angew. Chem. Int. Ed*. **37,** 550-575 (1998).

3. Xia, Y. & Whitesides, G. M. Soft Lithography. *Annu. Rev. Mater. Sci.* **28,** 153–184 (1998).

4. Kumar, A. & Whitesides, G. M. Features of gold having micrometer to centimetre dimensions can be formed through a combination of stamping with an elastomeric stamp and an alkanethiol "ink" followed by chemical etching. *Appl. Phys. Lett.* **63,** 2002–2004 (1993).

5. Lee, K.-B., *et al*. Protein nanoarrays generated by dip-pen nanolithography. *Science* **295,** 1702-1705 (2002).

6. Geissler, M. *et al*. Fabrication of metal nanowires using microcontact printing. *Langmuir* **19,** 6301–6311 (2003).

7. Hua, F., *et al*. Polymer imprint lithography with molecular-scale resolution. *Nano Letters* **4,** 2467-2471 (2004).

8. Nakagawa, T. *et al*. Fabrication of amino silane-coated microchips for DNA extraction from whole blood. *J. Biotechnol.* **116,** 105–111 (2005).

9. Sarveswaran, K., Hu, W., Huber, P.W., Bernstein, G. H. & Lieberman, M. Deposition of DNA rafts on cationic SAMs on silicon [100]. *Langmuir* **22,** 11279-11283 (2006).

10. Hidber, P. C., Helbig, W., Kim, E. & Whitesides, G. M. Microcontact printing of palladium colloids: micron-scale patterning by electroless deposition of copper. *Langmuir* **12,** 1375–1380 (1996).

11. Geissler, M., Kind, H., Schmidt-Winkel, P., Michel, B. & Delamarche E. Direct patterning of NiB on glass substrates using microcontact printing and electroless deposition. *Langmuir* **19,** 6283-6296 (2003).

12. Schreiber, F. Structure and growth of self-assembling monolayers. *Prog. Surf. Sci.* **65,** 151–256 (2000).

13. Flinck, S., Van Veggel, F. C. J. M. & Reinhoudt, D. N. Functionalization of self-assembled monolayers on glass and oxidized silicon wafers by surface reactions. *J. Phys. Org. Chem.* **14,** 407-415 (2001).

14. Onclin, S., Ravoo, B. J. & Reinhoudt, D. N. Engineering silicon oxide surfaces using self-assembled monolayers. *Angew. Chem. Int. Ed.* **44,** 6282-6304 (2005).

15. Wang, D., Thomas, S. G., Wang, K. L., Xia, Y. & Whitesides, G. M. Nanometer scale patterning and pattern transfer on amorphous Si, crystalline Si, and SiO_2 surfaces using self-assembled monolayers. *Appl. Phys. Lett.* **70,** 1593-1595 (1997).

16. Pompe, T., Fery, A. & Herminghaus, S. Submicron contact printing on silicon using stamps pads. *Langmuir* **15,** 2398-2401 (1999).

17. Ivanisevic, A. & Mirkin, C. A. "Dip-pen" nanolithography on semiconductor surfaces. *J. Am. Chem. Soc.* **123,** 7887-7889 (2001).

18. Jung, H., Kulkarni, R. & Collier, C. P. Dip-pen nanolithography of reactive alkoxysilanes on glass. *J. Am. Chem. Soc.* **125,** 12096-12097 (2003).

19. Kooi, S. E., Baker, L. A., Sheehan, P. E. & Whitman L. J. Dip-pen nanolithography of chemical templates on silicon oxide. *Adv. Mater.* **16,** 1013-1016 (2004).

20. Pena, D. J., Raphael, M. P. & Byers, J. M. "Dip-pen" nanolithography in registry with photolithography for biosensor development. *Langmuir* **19,** 9028-9032 (2003).

21. Hoff, J. D., Cheng, L.-J., Meyhöfer, E., Guo, L. J. & Hunt, A. J. Nanoscale protein patterning by imprint lithography. *Nano Letters* **4,** 853-857 (2004).

22. Maury, P., Péter, M., Mahalingam, V., Reindhoudt, D. N. & Huskens, J. Patterned self-assembled monolayers on silicon oxide prepared by nanoimprint lithography and their applications in nanofabrication. *Adv. Func. Mater.* **15,** 451-457 (2005).

23. Pallandre, A., Glinel, K., Jonas, A. M. & Nysten. B. Binary nanopatterned surfaces prepared from silane monolayers. *Nano Letters* **4,** 365-371 (2004).

24. Inoue, A., Ishida, T., Choi, N., Mizutani, W. & Tokumoto, H. Nanometer-scale patterning of self-assembled monolayer films on native silicon oxide. *Appl. Phys. Lett.* **73,** 1976-1978 (1998).

25. Sugimura, H., Nakagiri, N. & Ichinose, N. Area-selective formation of an organosilane monolayer on silicon oxide nanopatterns fabricated by scanning probe anodization. *Appl. Phys. Lett.* **66,** 3686-3688 (1995).

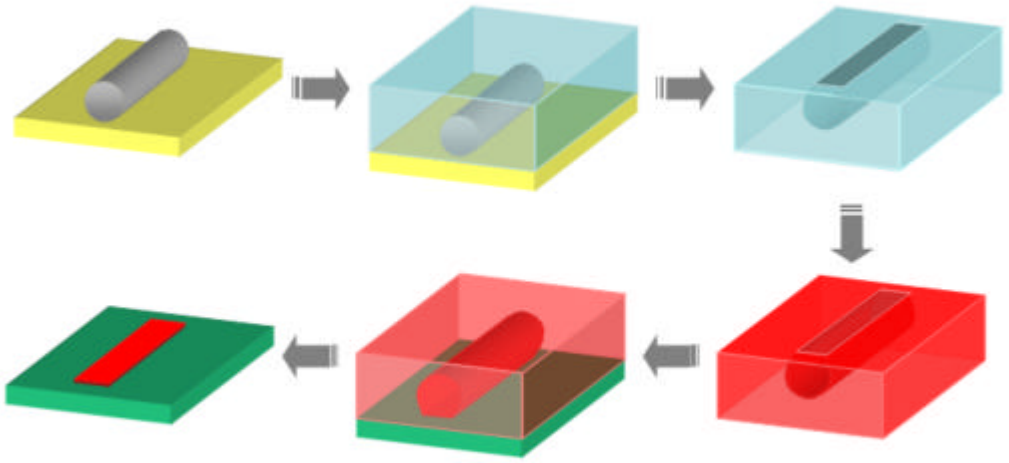

Figure 1. Scheme of the replica process. Clockwise: master, moulding, peeling, loading, transfer, replica.

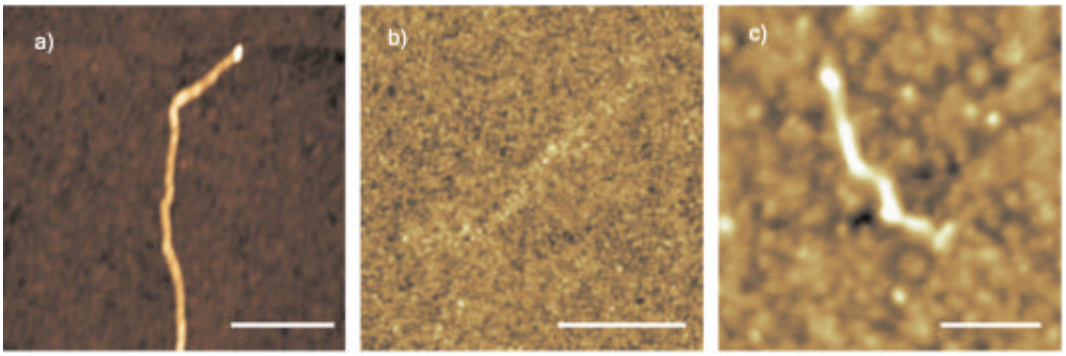

Figure 2. AFM images. a) Multi-walled carbon nanotube (scale bar: 400 nm), b) APTMS replica (scale bar: 500 nm), c) APTMS replica after site-specific oligonucleotide adsorption (scale bar: 150 nm).

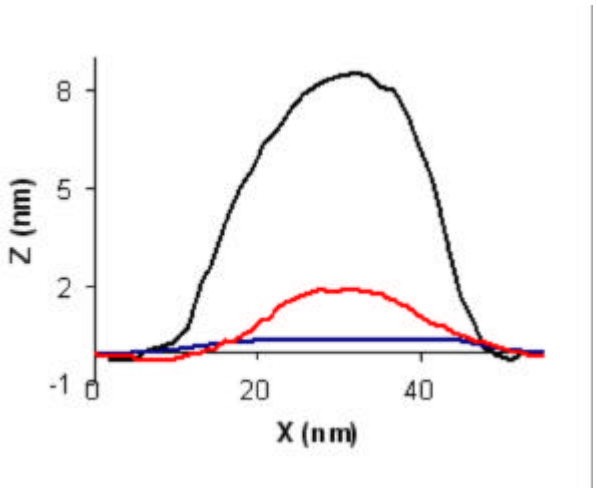

Figure 3. Cross sectional plots. Black: multi-walled carbon nanotube, blue: APTMS replica, red: APTMS replica after site-specific oligonucleotide adsorption.